



Large-scale opacity fluctuations in the Ly α forest: evidence for QSOs dominating the ionizing UV background at $z \sim 5.5\text{--}6$?

Jonathan Chardin,[★] Ewald Puchwein and Martin G. Haehnelt

Kavli Institute for Cosmology and Institute of Astronomy, University of Cambridge, Madingley Road, Cambridge CB3 0HA, UK

Accepted 2016 November 11. Received 2016 November 10; in original form 2016 June 27

ABSTRACT

Ly α forest data probing the post-reionization Universe show surprisingly large opacity fluctuations over rather large ($\geq 50 h^{-1}$ comoving Mpc) spatial scales. We model these fluctuations using a hybrid approach utilizing the large-volume Millennium simulation to predict the spatial distribution of QSOs combined with smaller scale full hydrodynamical simulation performed with RAMSES and post-processed with the radiative transfer code ATON. We produce realistic mock absorption spectra that account for the contribution of galaxies and QSOs to the ionizing UV background. These improved models confirm our earlier findings that a significant ($\gtrsim 50$ per cent) contribution of ionizing photons from QSOs can explain the large reported opacity fluctuations on large scales. The inferred QSO luminosity function is thereby consistent with recent estimates of the space density of QSOs at this redshift. Our simulations still somewhat struggle, however, to reproduce the very long ($110 h^{-1}$ comoving Mpc) high-opacity absorption through observed in ULAS J0148+0600, perhaps suggesting an even later end of reionization than assumed in our previously favoured model. Medium-deep/medium area QSO surveys as well as targeted searches for the predicted strong transverse QSO proximity effect would illuminate the origin of the observed large-scale opacity fluctuations. They would allow us to substantiate whether UV fluctuations due to QSO are indeed primarily responsible, or whether significant contributions from other recently proposed mechanisms such as large-scale fluctuations in temperature and mean free path (even in the absence of rare bright sources) are required.

Key words: methods: numerical – galaxies: evolution – quasars: general – cosmology: theory – diffuse radiation.

1 INTRODUCTION

The Ly α forest is the primary probe of the ionization state of hydrogen in the post-reionization Universe (see Becker, Bolton & Lidz 2015a for a recent review). The observed rapid rise in the mean flux level in Ly α forest data at $z < 6$ almost certainly marks the end of the reionization epoch (Fan et al. 2006; Becker et al. 2013; Becker et al. 2015b), while the rapid decline of the occurrence of Ly α emitters at $z > 7$ (Bolton & Haehnelt 2013; Dijkstra et al. 2014) and the rather low value of the Thomson optical depth suggested by recent *Planck* data (Planck Collaboration XIII 2016; Planck Collaboration XLVII 2016) point to a more rapid progress and a later start of the reionization of hydrogen than suggested by the early *WMAP* results. The Ly α forest data thereby do not only constrain when reionization ended, but may also provide important clues to the nature of the ionizing sources (see Theuns, Mo & Schaye 2001; Lidz et al. 2007; Wyithe, Bolton & Haehnelt 2008; Rorai,

Hennawi & White 2013; Kulkarni et al. 2015 and reviews of Ciardi & Ferrara 2005; Meiksin 2009; Becker et al. 2015a; McQuinn 2016).

The two types of ionizing sources considered to be most relevant during the reionization epoch are massive stars in star-forming galaxies and accreting supermassive black holes, while emission from accreting compact objects in binary stars is normally considered to be less important. More exotic sources, like decaying dark matter (DM) particles or evaporating primordial black holes have also been suggested to contribute to the ionizing photon budget. In recent years, most works in the field favour star-forming galaxies as the main driver of reionization. Their luminosity function is now well measured up to $z \sim 10$ (see Bouwens et al. 2015) down to a magnitude of $M_{\mathrm{AB}\,1600} \sim -16$. However, the fraction of radiation that actually escapes from star-forming galaxies into the intergalactic medium (IGM) f_{esc} is still poorly constrained. In the local Universe, only a few starburst galaxies are observed as Lyman continuum leakers with $f_{\mathrm{esc}} \leq 5$ per cent (see Borthakur et al. 2014; Leitherer et al. 2016). Efficient ionizing radiation leakers ($f_{\mathrm{esc}} \geq 10$ per cent) are more numerous at higher redshift (Reddy et al. 2016), but only a few are robust detections (Leethochawalit et al. 2016; Shapley

* E-mail: jc@ast.cam.ac.uk

et al. 2016). Overall, even at high redshift, the average escape fraction in all observations is still very small with $f_{\text{esc}} \leq 2$ per cent (Mostardi et al. 2015; Siana et al. 2015; Grazian et al. 2016). Recent numerical studies suggest that, on average, only ~ 10 per cent of the Lyman continuum photons escape from their host haloes in the mass range $10^8 M_{\odot} < M_{\text{halo}} < 10^{11} M_{\odot}$ (Kimm & Cen 2014; Ma et al. 2015; Xu et al. 2016). Only mini-haloes might reach high average escape fractions of $f_{\text{esc}} \sim 20\text{--}40$ per cent (Wise et al. 2014; Kimm et al. 2016; Xu et al. 2016), but it has been claimed that they would be a minor contributor to reionization as their star formation is inefficient (Kimm et al. 2016). Therefore, even for an optimistic assumption of $f_{\text{esc}} \sim 20$ per cent, the luminosity function of star-forming galaxies has to be extrapolated to faint magnitudes $M_{\text{UV}} \sim -13$ to provide enough ionizing photons to completely reionize the Universe by $z = 6$ (Robertson et al. 2013, 2015).

On the other hand, it has been claimed many times that emission from QSOs alone is likely not sufficient to reionize the Universe completely by $z = 6$ (see e.g. the pioneering work of Madau, Haardt & Rees 1999). In the last update of their model, Haardt & Madau (2012) argued once more that quasars alone would fail to reionize the Universe. The observations used to constrain the UV luminosity function of QSOs during reionization (Hopkins, Richards & Hernquist 2007) suggested an ionizing emissivity of QSOs well below the one required for reionization by $z = 6$ even assuming $f_{\text{esc}} = 1$. However, the observed QSO luminosity function at $z > 4$ is still rather uncertain, in particular, around the ‘knee’ of the luminosity function that should dominate the total ionizing emissivity from QSOs. The luminosity function used in calculations of the ionizing emissivity has therefore often been extrapolated from results at lower redshift. Recently, Giallongo et al. (2015) used an X-ray selection technique to provide a new observational estimate of the space density of faint QSOs in the CANDELS GOODS-S survey just at the tail end of reionization ($z \sim 5.75$). Surprisingly, they found that their estimated space density was significantly higher than most extrapolations of the QSO luminosity function from lower redshift. This led Madau & Haardt (2015) to reconsider the ionizing photon budget from QSOs, and they found that, if the increased ionizing emissivity suggested by Giallongo et al. (2015) can be extrapolated to higher redshift, QSOs could potentially reionize the Universe alone, even without a contribution from star-forming galaxies.

In a recent paper, Becker et al. (2015b, B2015 hereafter) presented detailed measurements of the probability distribution function (PDF) of the Ly α effective optical depth τ_{eff} averaged over scales of $50 \text{ cMpc } h^{-1}$ in the redshift range $4 \leq z \leq 6$ based on a sample of high S/N high-resolution QSO absorption spectra. B2015 found rather large fluctuations of the mean flux at $z > 5.5$. There are now five theoretical scenarios that have been suggested to explain the large scatter in the opacity distribution at the tail-end of reionization. First, B2015 argued that opacity fluctuations would result from fluctuations in the mean free path of ionizing photons just after percolation of H II regions. Secondly, right after B2015, Chardin et al. (2015) pointed out that fluctuations in the UV background from bright sources such as faint active galactic nuclei (AGNs) could cause the right amount of opacity fluctuations. Thirdly, D’Aloisio, McQuinn & Trac (2015) invoked large fluctuations of the temperature due to patchy reionization that could also lead to the observed opacity fluctuations. Fourthly, Davies & Furlanetto (2016) claimed that large-scale variations in the spatial distribution of the mean free path of ionizing photons in a galaxy only scenario would generate the right amount of fluctuations. Fifthly, recently, Gnedin, Becker & Fan (2016) argued that their set of radiation hydrodynamic simulations of reionization naturally gives the observed opacity

fluctuations when averaging multiple simulations with different initial conditions corresponding to different mean densities on the simulation box scale.

In the latter case, different reionization histories due to the different mean densities naturally lead to a level of scatter from line of sight to line of sight that matches the observed scatter. However, it is not clear that averaging from multiple simulations with different reionization histories is not introducing a bias in the results as the different simulated boxes evolve independently, while in reality underdense regions of the Universe may be reionized by neighbouring denser regions. Therefore, the results would likely differ from a single simulation with the same effective volume. The spatial variation of the mean free path case (B2015; Davies & Furlanetto 2016) is in tension with the scenario of D’Aloisio et al. (2015). Indeed, large values of the mean free path would be expected near overdensities containing many sources and much smaller values in voids far away from them. This would lead to high-transmissivity peaks in the Ly α forest near overdensities and to opaque segments in voids in these models. Conversely, in the temperature fluctuation model of D’Aloisio et al. (2015), we would expect colder regions near overdensities as those places are the first to reionize and have a longer time to cool after a passing ionization front. Thus, high-transmissivity peaks are expected far away from the galaxies, in voids that have been reionized at the end of the process. Finally, our model of UV background fluctuations due to rare bright sources would lie in the middle of the two latter scenarios. High-transmissivity regions are expected close to bright sources as in the fluctuating mean free path model but low-transmissivity regions could also occur near galaxy location that are far away from bright sources as in the temperature fluctuation model. Therefore, all the existing theoretical models lead to different observational signatures and forthcoming surveys could potentially discriminate between them. In the meantime, a more robust modelling is also required to provide guidance in interpreting the observational results.

Modelling the large-scale topology of reionization realistically is, however, very difficult due to the large dynamic range required (see Gnedin 2014; Gnedin & Kaurov 2014; Ocvirk et al. 2016 for recent ambitious attempts) and the numerically expensive coupling of radiative transfer effects and gas dynamics that is increasingly added to the simulations codes (see Rosdahl et al. 2013; Aubert, Deparis & Ocvirk 2015; Pawlik, Schaye & Dalla Vecchia 2015; Rahmati et al. 2015). Recently, we performed radiative transfer simulations of the reionization of hydrogen by (faint) galaxies in post-processing. They (marginally) resolve the sinks of ionizing radiation and show only rather moderate fluctuations of the UV background and the mean free path in the post-overlap phase of reionization (Chardin et al. 2015). As already said, this led Chardin et al. (2015) to suggest that much rarer brighter sources such as QSOs with space densities of $\sim 10^{-6} (\text{cMpc } h^{-1})^{-3}$ may contribute significantly to the ionizing background at $z \sim 5.5\text{--}6$ and be primarily responsible for the substantial opacity fluctuations at scales of $50 \text{ cMpc } h^{-1}$ and beyond at this redshift. We investigate here in detail the implications of this possible explanation of the large opacity fluctuations on large scales for the QSO luminosity function and the contribution of QSOs to the ionizing UV background at $z > 5$ (Georgakakis et al. 2015; Giallongo et al. 2015; Haardt & Salvaterra 2015; Madau & Haardt 2015; Fotopoulou et al. 2016; Matsuoka et al. 2016; Yoshiura et al. 2016).

This paper is organized as follows. In Section 2, we present our hybrid approach utilizing the large-volume Millennium simulation to model the spatial distribution of QSOs combined with smaller scale full hydrodynamical simulations performed with

RAMSES and post-processed with the radiative transfer code ATON. Section 3 presents our results with regard to spatial fluctuations of the photoionization rate and the corresponding opacity fluctuations in the Ly α forest. Section 4 discusses our work in the context of alternative models to explain the opacity fluctuations observed on large scales. We give our conclusions and outlook in Section 5.

2 METHODOLOGY

In this section, we will describe our modelling of the impact of large-scale fluctuations of the photoionization rate Γ on the PDF of the high-redshift Ly α optical depth. First, we will present briefly the main properties of the full (post-processed) radiative transfer hydrodynamical simulations used in our recent study (Chardin et al. 2015, hereafter Paper I). Then, we will describe our model of the spatial distribution of the contribution of QSO to the ionizing background based on a hybrid approach utilizing both the large-volume Millennium DM simulation (Springel et al. 2005) as well as our smaller volume full (post-processed) radiative transfer hydrodynamical simulations.

2.1 The radiative transfer simulations

2.1.1 The cosmological hydrosimulations

The simulations from Paper I are performed in two steps. First, hydrodynamic simulations are run. Then, in the second step the radiative transfer calculations are performed in post-processing on top of the hydrodynamic simulations adopting an ionizing source model.

The (cosmological) simulations of the evolution of the DM and the hydrodynamics of the gas were performed with the RAMSES code (Teyssier 2002). Note that we did not employ the adaptive mesh refinement option of RAMSES. We utilized a coarse, fixed grid discretized in 512^3 cells. The uniform UV background model of Haardt & Madau (2012; hereafter HM2012) was implemented in RAMSES to account for the photoheating of the gas. This gives a temperature evolution of the gas at mean density in reasonable agreement with recent observations of Becker et al. (2011) and Boera et al. (2014) (see fig. 3 of Paper I).

Note that our deliberately simplified simulations of the IGM also did not take into account supernova feedback and metal enrichment/cooling. As noted in Paper I, the lack of supernova feedback mainly affects the neutral hydrogen distribution in galactic haloes, which are too spatially concentrated to reproduce the observed incidence rate of dense absorbers.

2.1.2 Post-processed radiative transfer simulations with ATON

The radiative transfer calculations were performed in post-processing with the ATON code (Aubert & Teyssier 2008). ATON is a GPU-based radiative transfer code utilizing a moment-based description of the radiative transfer equation. We employed a monochromatic treatment that assumes all ionizing photons have an energy of 20.27 eV. The choice of energy of 20.27 eV is described in Baek et al. (2009). 20.27 eV is the mean energy of a 50 000-K blackbody spectrum that represents well the emission of ionizing photons of a population of stars with a Salpeter initial mass function in the mass range $1\text{--}100 M_\odot$. Adopting a different energy would only mildly affect the spatial distribution of the ionization fraction. A different photon energy will mainly affect the temperature calculations, as photons with a higher energy would heat the

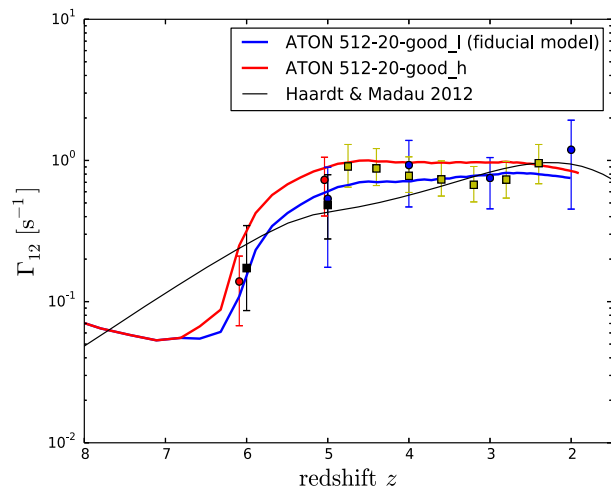


Figure 1. Redshift evolution of the average photoionization rate in already ionized regions (with an ionization fraction $x \geq 0.5$) in the full radiative transfer simulations from Paper I. The observational constraints shown with the different coloured symbols with error bars are from Bolton & Haehnelt (2007, blue), Calverley et al. (2011, red), Wyithe & Bolton (2011, black) and Becker & Bolton (2013, yellow).

gas more efficiently. However, the temperature calculation in our radiative transfer module is not used in our study. The temperatures are instead taken from the hydrosimulation performed with an HM2012 UV background accounting for the ionizing spectrum of galaxies and quasars. This results in a reasonable thermal history of the IGM compared to observations. Full radiative transfer ATON simulations were created based on snapshots of the optically thin RAMSES simulations separated by 40 Myr.

Ionizing sources were placed in the DM haloes identified in the RAMSES simulation and assumed to emit continuously. The ionizing luminosities were calibrated similarly as in Iliev et al. (2006) (but see also Chardin, Aubert & Ocvirk 2012; Chardin, Aubert & Ocvirk 2014) assuming a linear scaling of the ionizing luminosity with the mass of DM haloes. The normalization is thereby assumed to vary with redshift and is chosen so that the integrated comoving ionizing emissivity is roughly similar to that of the HM2012 uniform UV background model. Slight modifications were allowed so as to obtain an improved match of the hydrogen photoionization rates inferred from Ly α forest data.

In Fig. 1, we show $\Gamma_{12}(z) \equiv \Gamma(z)/10^{-12}$ for the ‘512-20-good_l’ and the ‘512-20-good_h’ models from Paper I that both agree well with the measured photoionization rates in the post-reionization Universe. In the acronyms, 512 denotes the resolution of 512^3 for the (coarse) grid while 20 stands for the box size of 20 comoving $Mpc h^{-1}$. In the particular case of these two simulations, ‘_l’ and ‘_h’ denote, respectively, ‘low’ and ‘high’, where low means a lower value of Γ_{12} and high a higher value of Γ_{12} at $z \sim 6$. In the rest of the paper, we will extensively use the ‘512-20-good_l’ model in our combined model of galaxies and AGNs, which we introduce in the next section.

2.2 A combined UVB model for galaxies and AGNs

In Paper I, we had seen that while our full radiative models of reionization by (faint) galaxies were able to reproduce the mean flux levels in the observed spectra, they did not reproduce the rather wide distribution of optical depths as measured by B2015 for $50 \text{ cMpc } h^{-1}$ chunks at $z > 5$. We thus investigated a simple

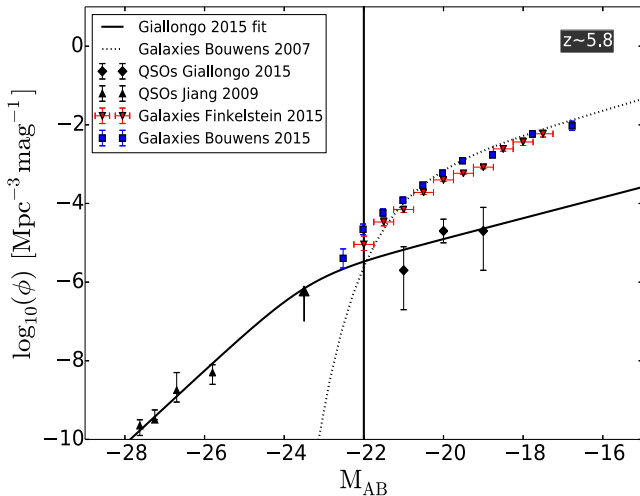


Figure 2. Fit to the QSO luminosity function (solid black) obtained by Giallongo et al. (2015) and a fit to the galaxy luminosity function (dotted black) obtained by Bouwens et al. (2007). For both QSOs and galaxies, observational constraints from a range of studies are shown according to the legend in the plot (Jiang et al. 2009; Bouwens et al. 2015; Finkelstein et al. 2015; Giallongo et al. 2015). The green cross shows luminosity and space density of the two bright sources in our model of the Ly α opacity PDF at $z = 5.8$ in Paper I.

toy model in which we assumed that a small number of bright sources assumed to be located in the most massive haloes of a 100^3 ($\text{Mpc } h^{-1}$) 3 DM simulation contribute to the ionizing UV background. We found that a model where about half of the ionizing UV background is due to bright ionizing sources with a space density of about 10^{-6} ($\text{cMpc } h^{-1}$) $^{-3}$ reproduces the PDF of the flux as measured by B2015 well.

We expand here on this by populating DM haloes in the Millennium simulation with bright sources (AGN) drawn from a model luminosity function. The latter is used to describe the UV luminosity of QSOs and their contribution to the ionizing emissivity. Its choice is guided by the observed space density of QSOs at these redshifts (see Fig. 2). We sort haloes by mass from the most massive to the least massive object and assign ionizing luminosities to them, which we draw from the model luminosity function in rank order (the most luminous ionizing source is placed in the most massive halo and so on). We then compute the photoionization rate Γ due to these bright sources at every position in the 500^3 ($\text{Mpc } h^{-1}$) 3 volume with the simple attenuation model used by B2015 (their galaxy UVB model of Section 4.2, but see also Bolton & Viel 2011; Viel et al. 2013).

In the calculation, we assume a spectral energy distribution appropriate for AGN for the bright sources of the form (see Vanden Berk et al. 2001; Telfer et al. 2002)

$$L_\nu \propto \begin{cases} \nu^{-0.44} & \text{if } \lambda > 1300 \text{ \AA} \\ \nu^{-1.57} & \text{if } \lambda < 1300 \text{ \AA} \end{cases} \quad (1)$$

This allows us to convert between the $L_\nu(1450)$ luminosities probed by observations and the ionizing luminosities governing the ionization state of the IGM.

At each spatial position, we compute the specific intensity of the ionizing background between 1 and 4 Ry by summing over the contribution from each bright source

$$J(\mathbf{r}, \nu) = \frac{1}{4\pi} \sum_{i=1}^N \frac{L_i(\mathbf{r}_i, \nu)}{4\pi|\mathbf{r}_i - \mathbf{r}|^2} e^{-\frac{|\mathbf{r}_i - \mathbf{r}|}{\lambda_{\text{mfp}}^{912}} \left(\frac{\nu}{\nu_{912}}\right)^{-3(\beta-1)}}, \quad (2)$$

where ν_{912} is the frequency at the H I ionizing edge and $\beta = 1.3$ is the slope of the H I column density distribution, which gives the dependence of mean free path on frequency (see also Songaila & Cowie 2010; Becker & Bolton 2013). The sum in equation (2) is performed for all sources within the simulation box and their periodically replicated images. In the following, we consider different constant values of the mean free path $\lambda_{\text{mfp}}^{912}$. Later on, we will allow it to spatially vary. The H I photoionization rate due to bright sources is computed as

$$\Gamma(\mathbf{r}) = 4\pi \int_{\nu_{912}}^{4\nu_{912}} \frac{d\nu}{h\nu} J(\mathbf{r}, \nu) \sigma_{\text{HI}}(\nu), \quad (3)$$

where $\sigma_{\text{HI}}(\nu)$ is the photoionization cross-section (calculated from the fit of Hui & Gnedin 1997).

As in Paper I, we then have investigated combining the photoionization rates due to bright sources in our model with the ionizing UV background due to the much more numerous galaxies driving reionization in our ATON simulations. We then calculated the expected effect of the rare bright sources on the Ly α opacity PDF in a model where both galaxies and QSOs contribute to the ionizing background.

We thereby combine the contributions from galaxies and QSOs as follows.

(i) We randomly choose a line of sight through the 500^3 ($\text{cMpc } h^{-1}$) 3 volume (along one of the principal axis) for which we have modelled the contribution of bright sources to the photoionization rate $\Gamma_{\text{QSO}}^{\text{fiducial}}$.

(ii) We concatenate three randomly selected line of sights from the ‘512-20-good_l’ full radiative transfer simulation and place them along the line of sight through the bright source model and call the photoionization rates due to the sources in the radiative transfer simulation $\Gamma_{\text{gal}}^{\text{fiducial}}$ and choose a mean free path.

(iii) We calculate the combined photoionization rates along the line of sight, $\Gamma_{\text{gal+QSO}} = \Gamma_{\text{gal}} + \Gamma_{\text{QSO}} = \beta_{\text{gal}} \Gamma_{\text{gal}}^{\text{fiducial}} + \beta_{\text{QSO}} \Gamma_{\text{QSO}}^{\text{fiducial}}$.

As we will see later, the contribution from galaxies is thereby poorly constrained by the PDF of the Ly α opacity as long as there is a significant contribution from QSOs. We will thus show results for two models bracketing the contribution of galaxies, one where we take into account all luminosities in our ‘fiducial’ ‘512-20-good_l’ model with a factor $\beta_{\text{gal}} = 1.0$. We also consider models with a slightly larger contribution from galaxies, $\beta_{\text{gal}} = 1.25$. We then determine the value of β_{QSO} by which we need to rescale the luminosities of the bright sources (QSOs) to match the PDF of the Ly α effective optical depth. For each model, for the spatial fluctuations of the photoionization rate, we calculate 5000 mock Ly α spectra for 50 cMpc h^{-1} chunks, i.e. using the same chunk size as in the observed sample of B2015, based on the density, temperature and peculiar velocity fields from the ‘512-20-good_l’ model (as e.g. described in Theuns et al. 1998).

2.3 Modelling UVB fluctuations due to bright sources (QSO)

2.3.1 The luminosity function of the bright sources (QSO)

We want to investigate here in particular whether QSOs drawn from a luminosity function at $z > 5$ consistent with the (still rather sparse) data at this redshift can produce sufficiently large spatial UVB fluctuations on large scales to reproduce the B2015 measurements. The recent observational constraints on the observed luminosity

Table 1. Parameters for the two-power law fit of the QSO luminosity function of equation (4) that fits the data of Giallongo et al. (2015). N_{QSO} is the number of QSOs above a limiting magnitude of $M_{\text{AB}} = -22$ in the $500^3 (\text{Mpc } h^{-1})^3$ volume of the Millennium simulations and ϵ_{912} is the corresponding comoving ionizing emissivity integrated over magnitudes brighter than $M_{\text{AB}} = -22$.

$\log_{10}(\phi^*)$	M_*	β	γ	N_{QSO}	$\epsilon_{912} (10^{24} \text{ erg s}^{-1} \text{ Hz}^{-1} \text{ Mpc}^{-3})$
-5.8	-23.4	1.66	3.35	1296	1.31

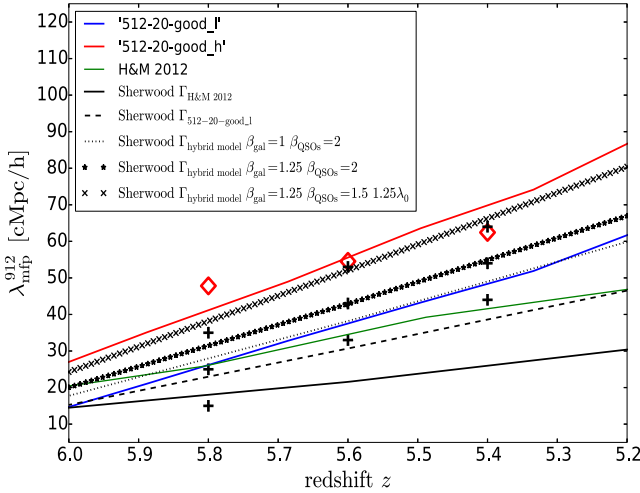


Figure 3. The range of mean free path values assumed in our models. The solid blue and red lines show, respectively, the evolution of the mean free path $\lambda_{\text{mfp}}^{912}$ in the reference models ‘512-20-good_l’ and ‘512-20-good_h’ as a function of redshift. The green line shows the evolution of $\lambda_{\text{mfp}}^{912}$ in the HM2012 model. The different black crosses show the values assumed in our different models with fixed mean free path. The open red diamonds show the extrapolation of the mean free path measured by Worseck et al. (2014) to higher redshift. The different black curves show the evolution of the mean free path in the Sherwood simulation for different values of the mean photoionization rate in the three redshift bins: assuming the HM2012 evolution (solid), assuming the mean Γ in our fiducial radiative transfer model ‘512-20-good_l’ (dashed) and using the converged value of $\langle \Gamma \rangle$ in our hybrid model (dotted).

function of Giallongo et al. (2015) can be reasonably fitted with a two-power law (see Fig. 2),

$$\phi^* = \frac{\phi}{10^{0.4(M_* - M)(\beta - 1)} + 10^{0.4(M_* - M)(\gamma - 1)}}, \quad (4)$$

with parameters M_* , β and γ as given in Table 1. We sample the luminosity function from the brightest luminosity present in our $500^3 (\text{cMpc } h^{-1})^3$ volume, which corresponds to $M_{\text{AB}} \sim -27$, and we adopt a lower limit of $M_{\text{AB}} = -22$ for the faintest QSOs and assume that the other QSOs with a fainter luminosity are part of the galaxy population. This results in 1296 QSOs in the $500^3 (\text{cMpc } h^{-1})^3$ volume.

2.3.2 The mean free path of ionizing photons

As we add the contribution of the UV background by QSO in a post-processing step, the next important parameter that we have to choose for the modelling of the spatial fluctuations of the ionizing UV background is the mean free path of ionizing photons due to QSOs. The solid blue and red curves in Fig. 3 show the evolution of the mean free path in our fiducial ‘512-20-good_h’ and ‘512-

Table 2. The range of $\lambda_{\text{mfp}}^{912}$ values investigated in our model with a constant mean free path for all the three redshift bins. The values of λ_0 and Γ_0 are the normalization used in equation (5) for our model with a Γ -dependent mean free path.

Redshift z	5.8	5.6	5.4
Fixed $\lambda_{\text{mfp}}^{912} (\text{cMpc } h^{-1})$	15,25,35	33,43,53	44,54,64
$\lambda_0 (\text{cMpc } h^{-1})$	18.0	21.6	26.0
$\Gamma_0 (\text{s}^{-1})$	2.95×10^{-13}	3.35×10^{-13}	3.74×10^{-13}

20-good_l’ full radiative transfer runs while the green fitted curve shows that assumed in the HM2012 UV background model (their best guess of extrapolating the mean free path observed at lower redshift to higher redshift). In the redshift range, we are interested in here, $z = 5.4\text{--}5.8$, the mean free path of ionizing photons is still rather uncertain and we have first explored a range of fixed values of mean free path spanning the range between that assumed by HM2012 and our fiducial radiative transfer simulations as shown by the small crosses in Fig. 3 and summarized in Table 2.

The highest values explored in each redshift bin are comparable with the extrapolation of measurements of the mean free path by Worseck et al. (2014) at lower redshift. The only exception is $z = 5.8$ where the values we consider are a bit lower. At this redshift, we are approaching the epoch of reionization where the mean free path is highly uncertain and could potentially strongly diverge from the extrapolation. The somewhat lower values we use are thus not implausible.

Assuming a fixed mean free path for the ionizing radiation of QSOs is obviously a rather poor approximation as the large UV fluctuations due to QSOs will also result in large fluctuations of the mean free path. Davies & Furlanetto (2016) based on the model of Miralda-Escudé, Haehnelt & Rees (2000) and the work of McQuinn, Oh & Faucher-Giguère (2011) argued that the mean free path in the post-reionization Universe should depend as a simple power law on the photoionization rate and density,

$$\lambda_{\text{mfp}}(\Gamma) = \lambda_0(\Gamma / \Gamma_0)^{2/3} \Delta^{-\gamma}. \quad (5)$$

Here, Δ is the overdensity in the simulation cells and γ sets the power-law dependence on the overdensity for the mean free path. Davies & Furlanetto (2016) choose a value of $\gamma = 1$, and we will investigate this model here as well as a model with a somewhat shallower dependence on overdensity (see Appendix A). As Γ itself will depend on the ionizing emissivity in these models as well as the mean free path, equation (3) has then to be solved iteratively.

For the normalization of the mean free path in equation (5), we have chosen λ_0 and Γ_0 such that we reproduce the mean free path in our numerical simulation in the limit of a spatially constant UV background.

To this end, we have measured the mean free path in the 40-2048-ps13 run of the Sherwood Simulation Suite (Bolton et al. 2017) using the method described in appendix C of Paper I and applying the Rahmati et al. (2013) self-shielding prescription. The simulation assumes an HM2012 UV background and includes a wide range of galaxy formation physics (Puchwein & Springel 2013). The mean free path is averaged over many random lines of sight. We then adopt the measured mean free path as λ_0 and the assumed photoionization rate from HM2012 as Γ_0 . The corresponding values for λ_0 and Γ_0 are reported in Table 2 for the three redshift bins considered. We have also tested by rescaling the ionized fractions to a different photoionization rate and by selecting lines of sight with a suitable smoothed overdensity at the starting point that equation (5)

faithfully describes the scaling of the mean free path with Γ and Δ . A value of $\gamma \approx 0.4$ is preferred by this comparison, but larger values of γ up to unity are obtained when measuring the mean absorption over short path lengths.

Note that in our Γ -dependent model for the mean free path we have also iteratively accounted for the expected dependence of the photoionization rate due to galaxies on the mean free path by modulating the photoionization rate predicted by our full radiative transfer simulation accordingly,

$$\Gamma_{\text{gal}}^{\text{fiducial}}(\Gamma_{\text{gal+QSO}}) = \Gamma_{\text{gal RT}} \frac{\lambda_{\text{mfp}}(\Gamma_{\text{QSO+gal}})}{\lambda_{\text{mfp}}(\Gamma_{\text{gal RT}})}, \quad (6)$$

where $\Gamma_{\text{gal RT}}$ is the photoionization rate due to galaxies in the radiative transfer simulation at a given location, and we have assumed the galaxy mean free path to scale with photoionization rate and overdensity as in equation (5).

3 RESULTS

3.1 Spatial fluctuations of the photoionization rate distribution in the full radiative transfer simulations

First, we look at the spatial distribution of the photoionization rate Γ in our full radiative transfer simulations at different redshifts. Fig. 4 shows the redshift evolution for our fiducial ‘512-20-good_l’ simulation. As expected before overlap of the H II regions, there are large spatial variations but as discussed in Paper I these damp out very quickly after overlap of the H II regions that occurs at $z = 6.5$ –6 (see fig. 11 of Paper I for the redshift evolution of the PDF of Γ_{12}). At $z = 5.9$, the photoionization rate in our fiducial simulation is already very homogeneous, but see Davies & Furlanetto (2016) for a discussion how the rather small volume covered by our simulations may affect the amplitude and scale of spatial fluctuations of the photoionization rate. Note, however, that we did not see any large effect of the box-size of our simulations in Paper I.

3.2 Spatial fluctuations of the photoionization rate in our combined UVB model of (faint) galaxies and QSOs

Fig. 5 shows maps of the photoionization rate Γ_{gal} and Γ_{QSO} at $z \sim 5.8$ assuming a fixed mean free path. The maps shown are the ones that best match the observed cumulative Ly α effective optical depth PDF as explained in Section 3.3.

For the fit to the QSO luminosity function as in Giallongo et al. (2015), the luminosities need to be rescaled by a factor $\beta_{\text{QSO}} = (16, 8, 5)$ in order to match the observed Ly α effective optical depth PDF at redshift $z = 5.8$ for our models with mean free path of (15, 25, 35) cMpc h^{-1} . These rather high values of β_{QSO} are due to the fact that our assumed mean free path is lower than the (mean) distance between the QSOs in our model. As already discussed neglecting the effect of the QSOs on the mean free path is a bad approximation. As we will see the required luminosities to match the PDF are significantly lower for our more realistic models with a Γ -dependent mean free path. The upper-right panel shows the effect of introducing a Γ -dependent mean free path as described in Section 2.3.2. In this case, the value of β_{QSO} decreases to ~ 1.5 –2 and the luminosity function required to reproduce the observed opacity fluctuations gets close to that observed by Giallongo et al. (2015). As we will discuss later, this agreement should improve further if the expected increase of the temperature in the proximity of the QSO due to ionization of He II would be taken into account. This is currently neglected in our simulations.

3.3 Opacity fluctuations in the Ly α forest in the combined UVB model of (faint) galaxies and QSOs

Here, we present in Fig. 6, the cumulative Ly α optical depth PDFs of our mock absorption spectra for the different models. We choose to show the cumulative rather than the differential PDFs as the former were discussed in the original observational paper of B2015. We have shown in Paper I that for the case of a galaxy only model (i.e. $\beta_{\text{QSOs}} = 0$) the Ly α optical depth PDFs are too steep and cannot explain the observed scatter. As already mentioned in the last section, we are able to match the τ_{eff} PDF in all redshift bins with our combined model of galaxies and QSOs. In each panel, the yellow curves show 30 different realizations of the PDF computed with the same path length as in the B2015 sample in the corresponding redshift bins. In every model, the scatter of the PDF brackets the observations reasonably except perhaps the high opacity point in the redshift bin $z = 5.6$. We should note here that these large optical depths can all be traced to the very long ($110 h^{-1}$ cMpc) trough in ULAS J0148+0600. If we allow for a rescaling of the luminosities, matching the PDF is not very difficult, but the amount by which we have to rescale the photoionization rate Γ of the QSO counterpart in order to get agreement with the observations is rather different from one model to another. In each panel, we show the β_{QSOs} values we need to match the PDF for a fixed $\beta_{\text{gal}} = 1$. The β_{QSOs} values were found by testing qualitatively how well different values reproduce the observed opacity PDFs.

In Fig. 6, we show the effect of varying the assumed (spatially constant) mean free path. We can see that changing the mean free path moderately changes the shape of the PDF in all the redshift bins, especially for the two lower redshifts $z = 5.6$ and $z = 5.4$. With increasing mean free path, the opacity PDF becomes narrower, while the ionizing emissivity and to a smaller extent the contribution to the photoionization rate from QSOs required to match the observed PDF decreases. Similar conclusions have been reported by B2015. Lowering the mean free path leads to larger photoionization rate fluctuations as the low-density IGM would see less and less ionizing photons.

Let us now have a look at the effect of introducing a spatially varying mean free path. In Fig. 7, we compare the Ly α effective optical depth PDF for the case of a constant mean free path and with a set of Γ -dependent mean free path parametrization as described in Section 2.3.2. As already mentioned, the value of β_{QSOs} decreases to 1.5–2 with the Γ -dependent mean free path parametrization at $z = 5.8$ if we assume the mean free path to depend on overdensity as Δ^{-1} . Large values of the mean free path close to ionized regions have the effect of increasing the $\langle \Gamma_{\text{QSOs}} \rangle$ values. Therefore, for a given luminosity function, adopting a photoionization-dependent mean free path parametrization in the combined UVB model leads to a lower value of β_{QSOs} required to generate photoionization rate fluctuations that match the PDF of τ_{eff} .

A weaker dependence of the mean free path on overdensity as $\Delta^{-0.4}$ as suggested by our measurements of the mean free path in the Sherwood simulation leads to similar values of β_{QSOs} needed to match the τ_{eff} PDF. The overdensity dependence of the mean free path seems therefore to play only a minor role for the resulting UV background and the related τ_{eff} PDF. We have also tested different smoothing scales for the overdensity field Δ measured from the Millennium simulation. This also changes our results very little (see Appendix A).

We should, however, note that for models with the original luminosity function of Giallongo et al. (2015) ($\beta_{\text{QSOs}} = 1$), the τ_{eff} values are somewhat high compared to the data of B2015. We

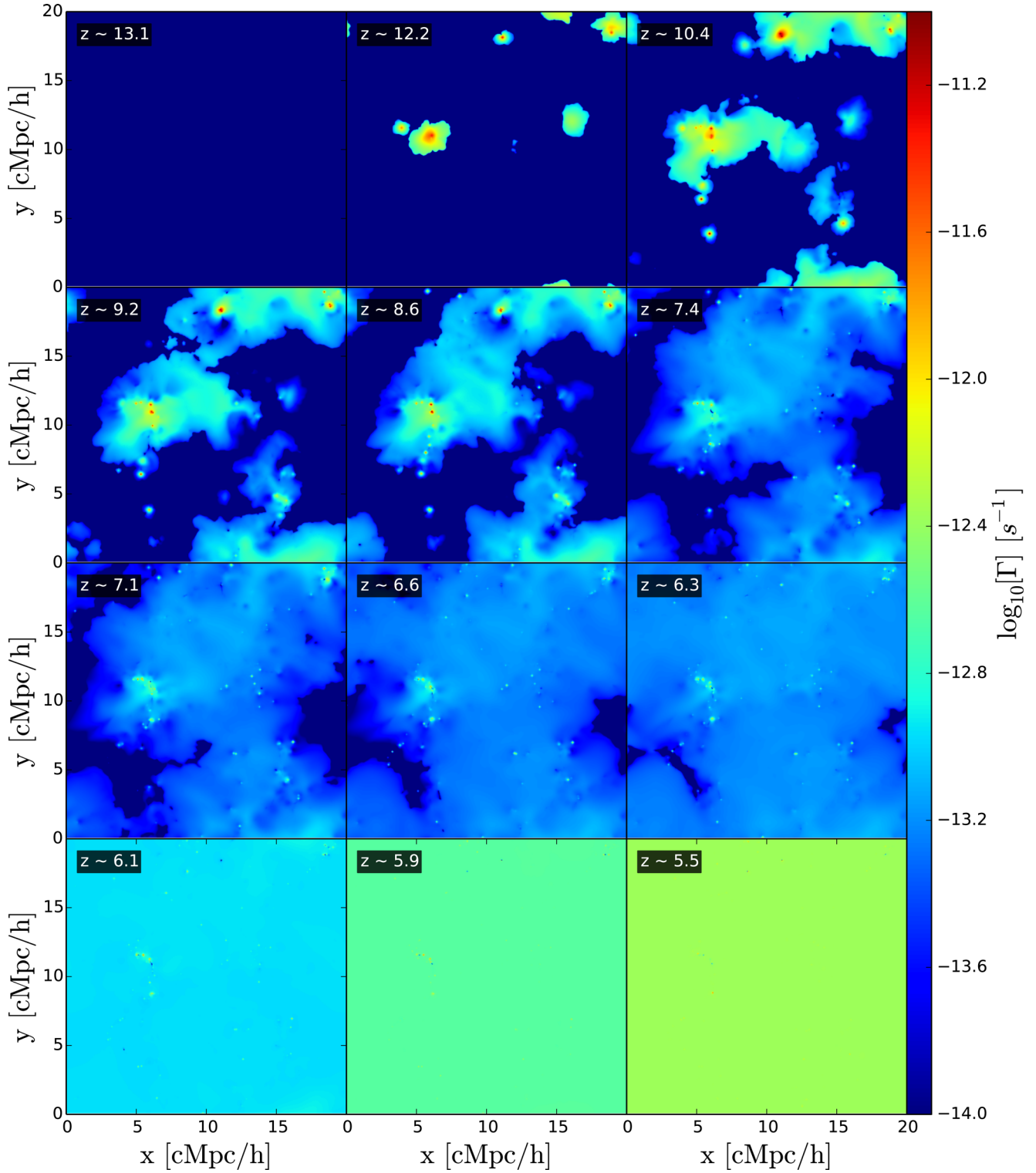


Figure 4. Redshift evolution of the spatial distribution of Γ in our fiducial ‘512-20-good_l’ full radiative transfer simulation in a slice of thickness $39.0625 \text{ ckpc } h^{-1}$.

therefore had a closer look at the data of B2015 and noted that there is a noticeable offset between the PDF reported by B2015 based on their own sample of QSO spectra combined with the sample of Fan et al. (2006) compared to the PDF for the B2015 sample only (shown as the dotted step function in Fig. 7). The latter is indeed preferring models with a somewhat lower photoionization rate. This

offset is somewhat larger than could be due to statistical fluctuations for samples of this size. We convinced ourselves that at least part of the difference could be due to a more conservative cleaning of B2015 of their own sample for regions where the observed flux is affected by proximity effects of the observed QSOs (caused by their ionizing flux and to a lesser extend the matter clustering around

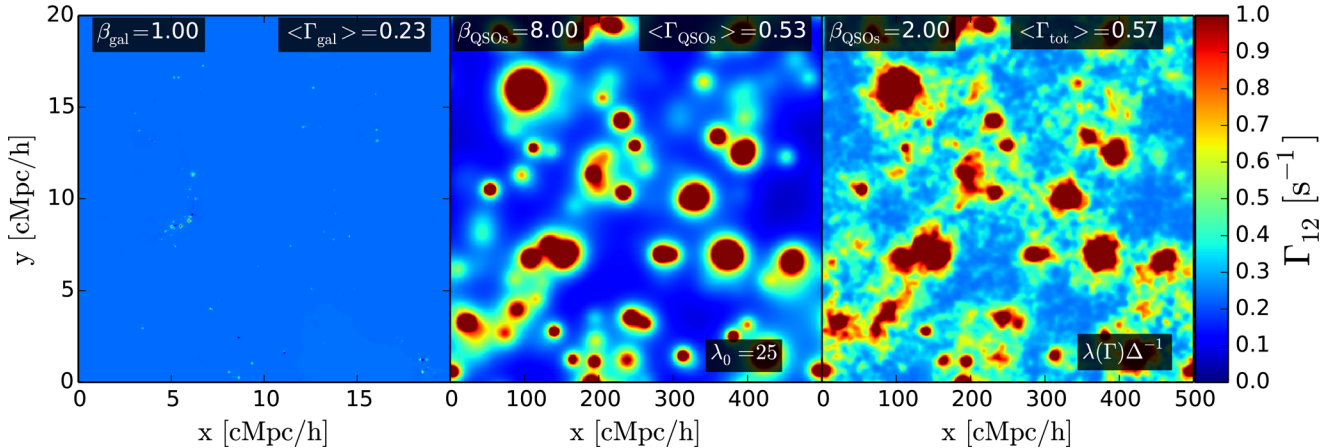


Figure 5. Left: spacial distribution of the photoionization rate Γ_{12} in a slice of $39.0625 \text{ ckpc } h^{-1}$ thickness through our fiducial $20 \text{ Mpc } h^{-1}$ radiative transfer simulation ('512-20-good_l') at redshift $z \sim 5.8$ (galaxies only). Middle: spatial distribution of the photoionization rate (Γ_{12}) due to QSOs in a slice of $976.5625 \text{ ckpc } h^{-1}$ through the Millennium simulation at redshift $z \sim 5.8$ for a constant mean free path of $\lambda_0 = 25 \text{ cMpc } h^{-1}$. Right: spatial distribution of the photoionization rate due to QSOs plus galaxies (Γ_{12}) for a Γ -dependent parametrization of the mean free path $\lambda(\Gamma)$ according to equation (5) with $\lambda_{\text{mfp}} \propto \Delta^{-1}$. The mean photoionization rate $\langle \Gamma \rangle$ reported in the upper-right corner of the left-hand panel is that due to galaxies only in our fiducial full radiative transfer simulation and that in the middle panel is that due to the additional QSOs contribution β_{QSOs} necessary to match the Ly α opacity PDF with a fixed mean free path of $\lambda_0 = 25 \text{ Mpc } h^{-1}$.

them). The size of the proximity regions is strongly dependent on the assumed photoionization rate due to surrounding galaxies and therefore not straightforward at these redshifts.

3.4 The lengths of Gunn–Peterson troughs

As we have seen reproducing the large opacity fluctuations reported by B2015 on large scales ($\gtrsim 50 \text{ } h^{-1} \text{ cMpc}$) is difficult and the very long ($110 \text{ } h^{-1} \text{ cMpc}$) high-opacity trough in ULAS J0148+0600 is particularly challenging. The box sizes of our high-resolution hydrosimulation are significantly smaller than this, but the scale of the opacity fluctuation in our model is set by the UV fluctuations due to the proximity effect that we model as before with the $500^3 (\text{Mpc } h^{-1})^3$ Millennium simulation.

In order to see if we are able to reproduce such a long high-opacity trough in our hybrid simulations we proceeded as follows.

- (i) We choose a random line of sight through the $(500 \text{ Mpc } h^{-1})^3$ Millennium volume along one of the principal axis.
- (ii) We calculate the $\Gamma_{\text{QSO}}^{\text{fiducial}}$ values due to QSOs along that skewer discretized in $500/20 \times 512$ cells with equation (3).
- (iii) We concatenate $500/20 = 25$ randomly selected line of sights from the '512-20-good_l' model and place them along the $500 \text{ Mpc } h^{-1}$ skewer through the Millennium simulation.
- (iv) We calculate the combined photoionization rates along the line of sight, $\Gamma_{\text{gal+QSO}} = \Gamma_{\text{gal}} + \Gamma_{\text{QSO}} = \beta_{\text{gal}} \Gamma_{\text{gal}}^{\text{fiducial}} + \beta_{\text{QSO}} \Gamma_{\text{QSO}}^{\text{fiducial}}$.
- (v) We repeat this procedure for 500 random skewers through the $500 \text{ Mpc } h^{-1}$ Millennium simulation. From each of the 500 skewers, we pick randomly five $110 \text{ Mpc } h^{-1}$ chunks and calculate the effective optical depth from mock absorption spectra, resulting in 2500 estimates of τ_{eff} .

We use here again our simulation with the QSO luminosity function of Giallongo et al. (2015) at $z = 5.8$ with $\beta_{\text{gal}} = 1$ and $\beta_{\text{QSOs}} = 2$ for the Γ -dependent mean free path case with an over-density dependence as Δ^{-1} . We note that the over-density field Δ of the Millennium simulation has been smoothed here on 20 cMpc scale to calculate the photoionization rate values.

In Fig. 9, we show 10 examples of our mock spectra for a range of effective optical depth values and in the top and bottom-right panels of Fig. 8 the corresponding line of sights are overlaid on maps of the photoionization rate Γ and the optical depth τ of our hybrid simulations. The top and bottom-left panels of Fig. 8 show the DM overdensity of the corresponding slice of the Millennium simulation and the hydrogen density in the concatenated high-resolution hydrosimulations, respectively. For each mock absorption spectrum in Fig. 9, the τ_{eff} computed in a $110 \text{ Mpc } h^{-1}$ portion of the skewer marked in blue is given. We indeed find a few spectra with $\tau_{\text{eff}} > 7$ as measured for the long trough in ULAS J0148+0600.

Fig. 10 shows the cumulative PDF of τ_{eff} inside skewers computed from the 500 mock Ly α spectra. We show the PDF for three different lengths for which τ_{eff} values are calculated. The vertical line in the figure shows $\tau_{\text{eff}} = 7$, the value reported by B2015 for ULAS J0148+0600, while the horizontal lines show fractions of 10, 1 and 0.1 per cent.

There is a non-negligible tail of the PDF at $\tau_{\text{eff}} > 7$ for $\Delta_l = 10$ and $50 \text{ Mpc } h^{-1}$ with, respectively, about 30 per cent and 7 per cent of the line-of-sight chunks that lie above this value for our model with $\beta_{\text{QSOs}} = 2$ and $\beta_{\text{gal}} = 1$. Somewhat surprising this is in reasonable agreement with the recent finding of Gnedin & Kaurov (2014) who found a value of about 3 per cent of their line of sights (computed in $40 \text{ Mpc } h^{-1}$ chunks) that have $\tau_{\text{eff}} > 7$ at $z \sim 5.8$ in their full hydro-RT simulation that do, however, not contain UV fluctuations due to QSOs. There is also a small number of line of sights that have $\tau_{\text{eff}} > 7$. For $\Delta_l = 110 \text{ cMpc } h^{-1}$, 10 per cent of chunks of our mock spectra have $\tau_{\text{eff}} > 6$ and about 2 per cent have $\tau_{\text{eff}} > 7$ as in the observed very long trough in ULAS J0148+0600. Since the Ly α forest part of the spectrum of a $z \sim 6$ QSO extends about $370 \text{ cMpc } h^{-1}$, we predict an ~ 7 per cent chance of it containing such a long absorption trough. The fraction of such spectra drops, however, rapidly if we increase β_{gal} suggesting that reionization by galaxies occurs as late or later as in our fiducial 512-20-good_l full radiative transfer simulation.

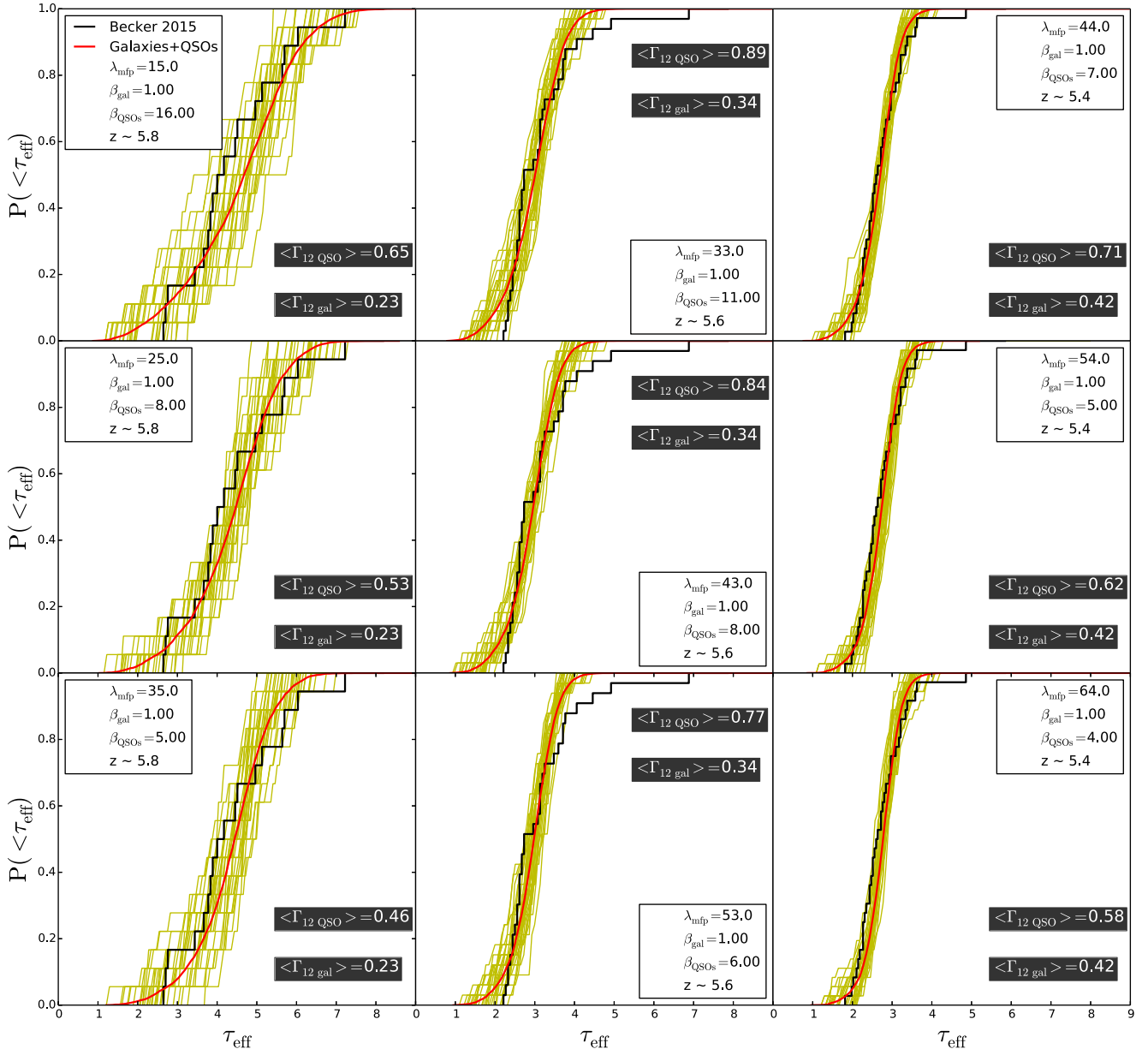


Figure 6. PDF of τ_{eff} for the rescaled luminosity functions with the same shape as the fit in Giallongo et al. (2015) and different fixed mean free paths at the three different redshifts (first column: $z \sim 5.8$, second column: $z \sim 5.6$, third column: $z \sim 5.4$). The different constant mean free paths considered at the three redshifts are ($z \sim 5.8$: 15,25,35 cMpc h^{-1} , $z \sim 5.6$: 33,43,53 cMpc h^{-1} , $z \sim 5.4$: 44,54,64 cMpc h^{-1}) as discussed in Section 2.3.2.

Comparing the individual spectra with the lower panels of Fig. 8 is rather illustrative. Individual regions of high transmitted flux can be clearly traced back to the transverse proximity effect due to the corresponding line of sight passing rather close to a QSO. This is a clear observational prediction of the model but relies crucially on the assumed long-lifetimes of the QSO and isotropic nature of their emission. Unfortunately, failure to find easily the signature of a transverse proximity effect will therefore not necessarily rule out the QSO proximity effect as a source of the opacity fluctuations. Instead, it will put limits on the duty cycle and angular distribution of the emission of QSOs. Interestingly, Gallerani et al. (2008) have already reported the detection of a transverse proximity effect at $z = 5.70$ in the Ly α forest part of the spectrum of SDSSJ1148+5215.

4 DISCUSSION

4.1 Are there a sufficient number of QSOs?

As we had seen the required contribution by QSOs to the ionizing emissivity is model dependent and depends in particular on the modelling of the mean free path for ionizing photons. This is still very difficult to do self-consistently as full radiative transfer simulations including QSO with sufficient dynamic range to properly resolve the sinks of reionization/Lyman-limit systems are not yet possible. For our most realistic model of a Γ -dependent mean free path calibrated with a high-dynamic range hydrodynamical simulation, QSOs drawn from a luminosity function as measured by Giallongo et al. (2015) appear to be just about sufficient to explain the observed opacity fluctuations on large scales given the

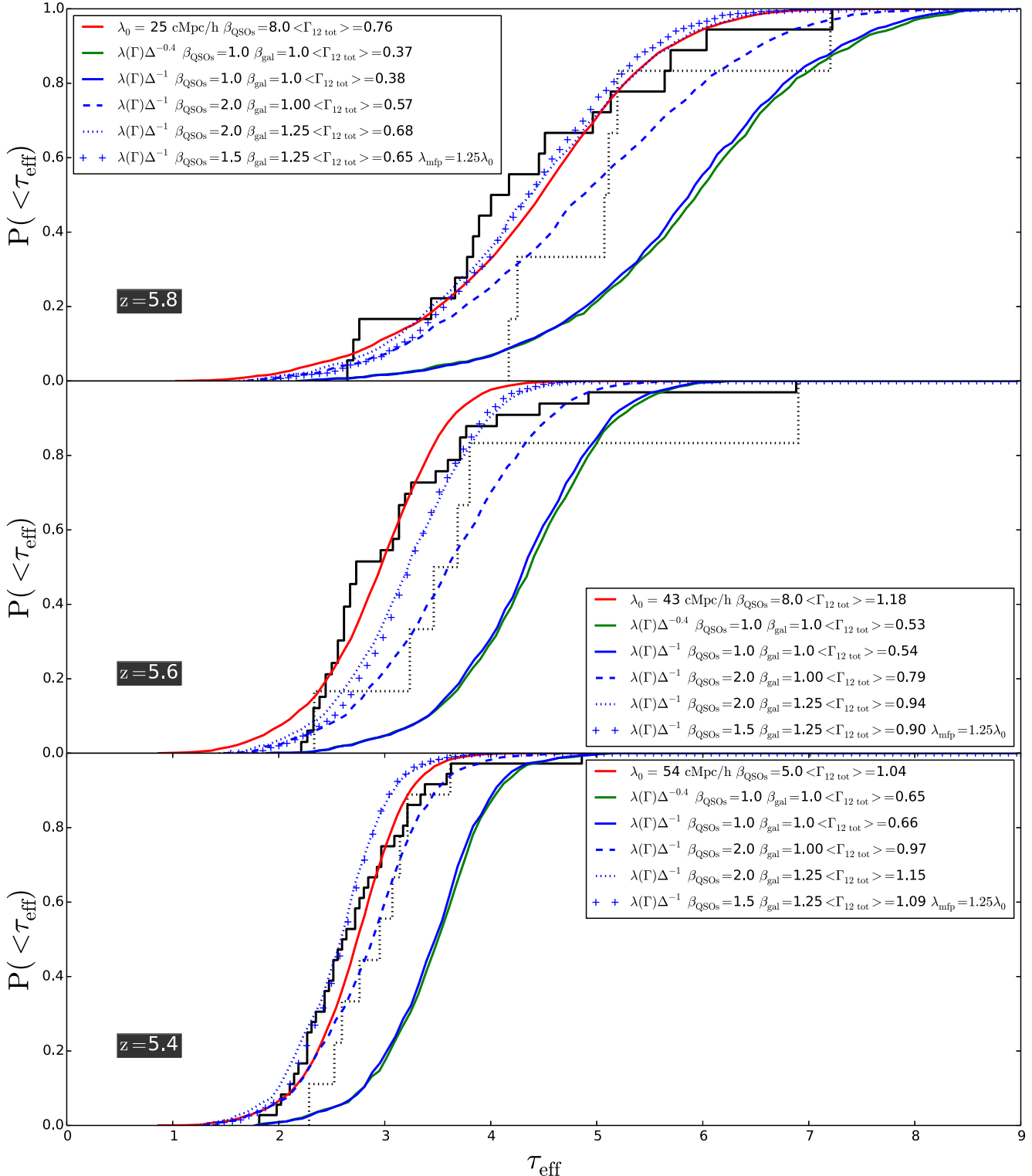


Figure 7. PDF of τ_{eff} for models with the (rescaled) luminosity function of Giallongo et al. (2015) at the three redshifts with values β_{gal} and β_{QSOs} as indicated in the plots. The red curves shows the case with a constant mean free path $\lambda_{\text{mfp}} = \lambda_0$ while the other solid coloured curves show cases with a varying mean path adopting the different parametrization chosen in equation (5). The black solid step function shows the data from B2015 based on their own sample of QSO spectra combined with the sample of Fan et al. (2006) while the dotted black step function is for the B2015 sample only.

uncertainties in both the modelling and the data. Note, in particular, that we have not taken into account in our modelling the effect of the additional photoheating due to the harder spectra of the QSOs, which will lead to an earlier reionization of He II in

the vicinity of the QSOs. This should lead to temperature fluctuations on comparable spatial scales and would lead to an amplification of the opacity fluctuations as low-opacity regions would also be hotter and therefore have a reduced recombination rate

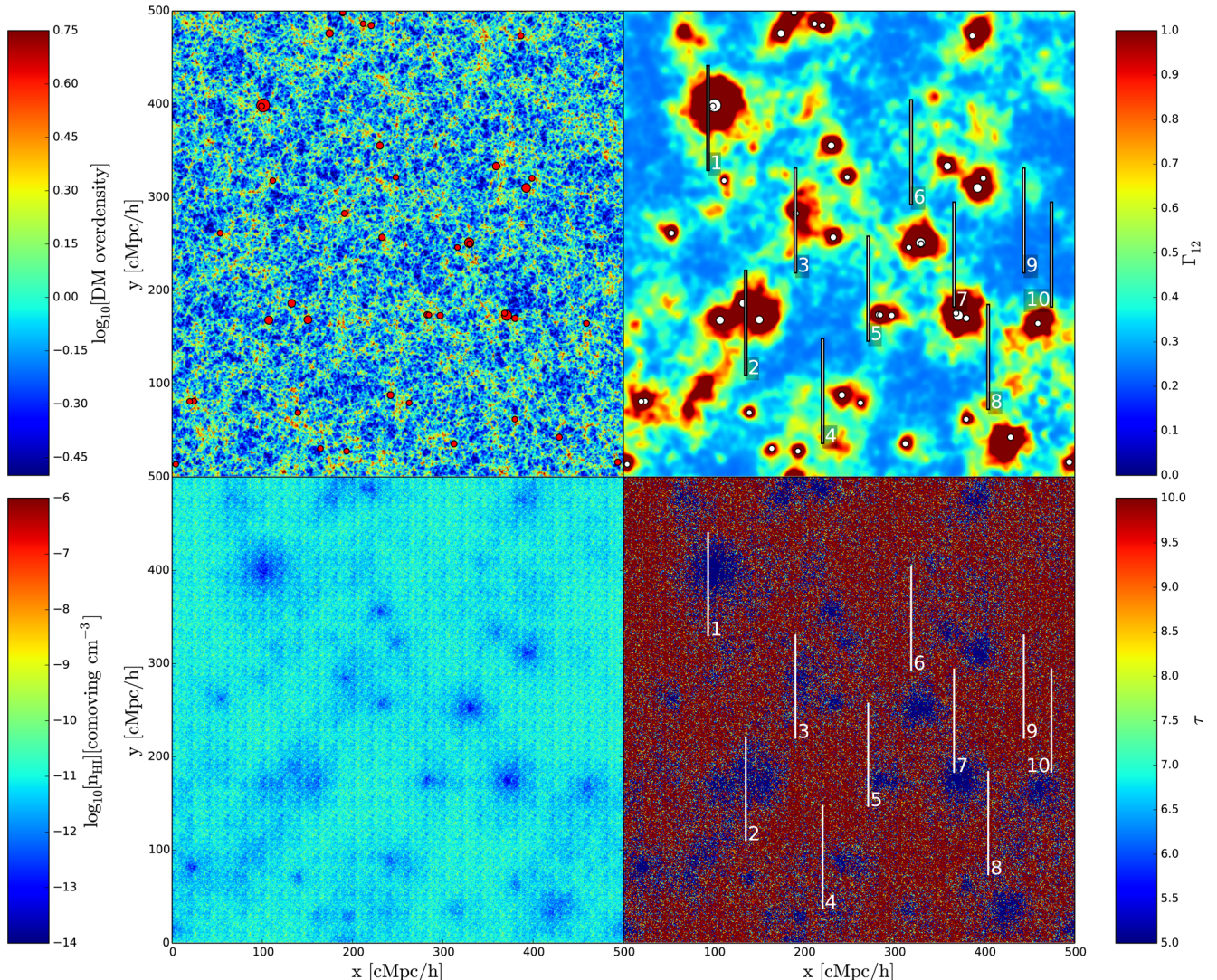


Figure 8. Top left: spatial distribution of the DM overdensity in the Millennium volume at $z \sim 5.8$ in a slice of thickness $976.6 \text{ ckpc } h^{-1}$. The red circles show the location of the DM haloes hosting the QSOs. Top right: the spatial distribution of the photoionization rate Γ_{12} in the volume of the Millennium volume simulation for the fit of the QSO luminosity function of Giallongo et al. (2015) with the Γ -dependent mean free path case, $\lambda_{\text{mfp}} = \lambda_0(\Gamma/\Gamma_0)^{2/3} \Delta^{-1}$. The map has been calculated for a 512×512 grid and then interpolated on a 4096×4096 grid. The overdensity field Δ from the Millennium simulation has been smoothed on a 20 cMpc scale with a top-hat filter to calculate the Γ_{12} field in the slice. Bottom left: the spatial distribution of the neutral hydrogen number density inside the Millennium volume: the density field in the mid-plane slice of the '512-20' RAMSES simulation is replicated 25×25 to cover the full size of the Millennium simulation and has been interpolated on a 4096×4096 grid. Bottom right: the spatial distribution of the opacity τ in the same slice calculated using the interpolated 4096×4096 grids of the hydrogen number density (bottom-left panel), velocity (not shown in the plot), temperature (not shown in the plot) and photoionization rate (top-right panel). The red and white points, respectively, in the upper- and bottom-left panels show the position of the DM haloes assumed as ionizing sources in our model (taken in a slice of $\sim 15 \text{ cMpc } h^{-1}$ thickness around the slice shown). The black/white thick lines in the bottom-left/right-hand panel show 10 lines of sight of $110 \text{ Mpc } h^{-1}$ length along which we compute and show the corresponding spectra in Fig. 9. The maps shown are calculated with $\beta_{\text{QSOs}} = 2$ and $\beta_{\text{gal}} = 1$.

further reducing the opacity. Taking this into account should reduce the contribution of QSO to the ionizing emissivity required to produce the same level of opacity fluctuations. This may be necessary if the contribution of QSO to the ionizing emissivity is lower as suggested by the luminosity function measured by Giallongo et al. (2015), what may – as discussed in the Introduction – well be the case. We have also not accounted for a possible beaming and/or (short) duty cycle of the QSOs in our modelling and the net effect of these on the predicted opacity fluctuations is not obvious.

4.2 Alternative models for the large opacity fluctuations on large scales

We have shown here that large amplitude UV background fluctuations due to a significant contribution of QSOs may be able to explain the large reported opacity fluctuations. A similar conclusion has been reached by D'Aloisio et al. (2016), which first became available to us during the refereeing process of this paper. However, it is not certain that QSOs in sufficient numbers actually exist. We therefore briefly discuss here also alternative suggestions. Davies & Furlanetto (2016) presented modelling where

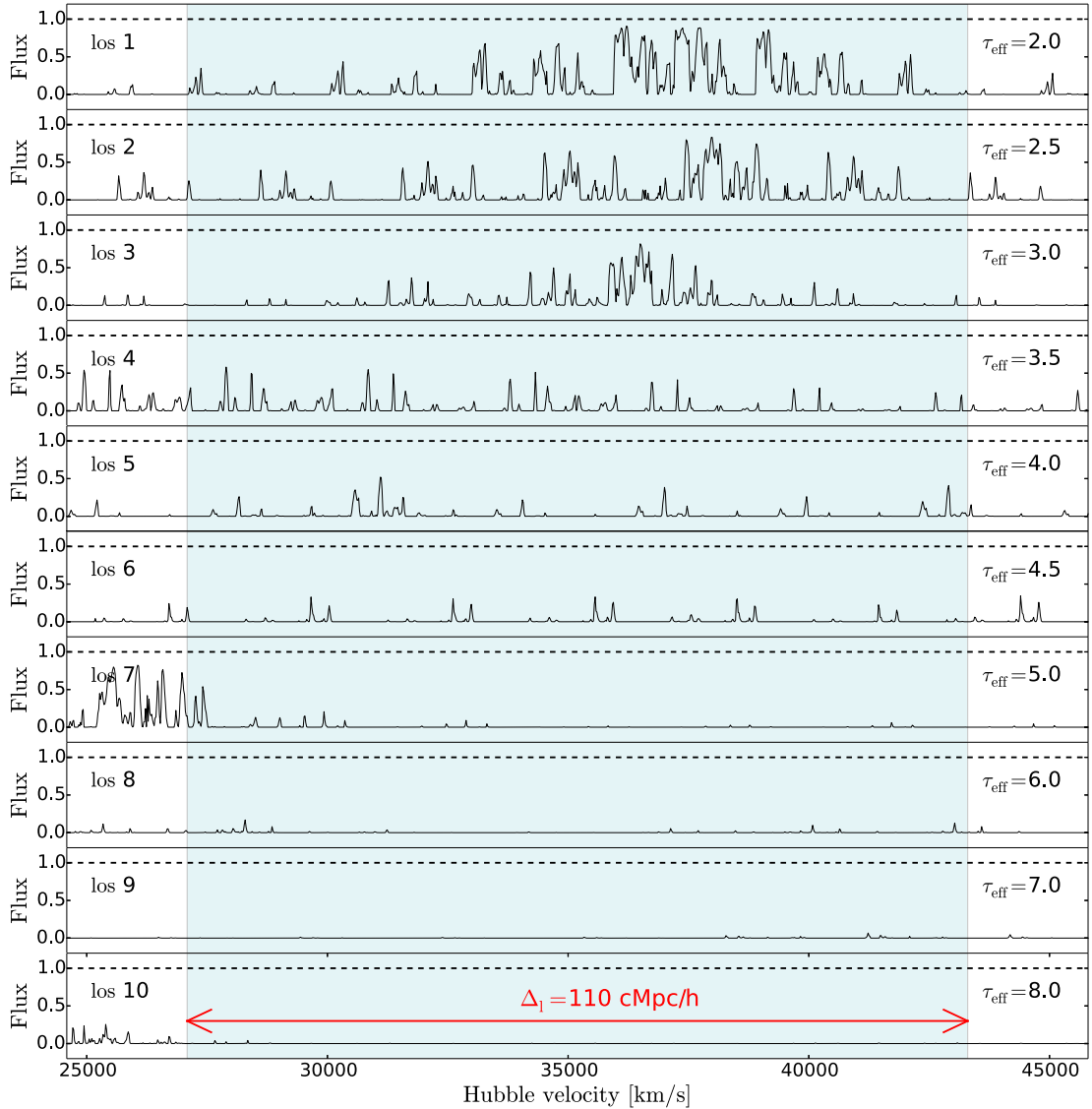


Figure 9. Example of 10 spectra obtained along one of the principal axis at $z = 5.8$ for our model with the luminosity function of Giallongo et al. (2015) and with a varying mean free path: $\lambda_{\text{mfp}} = \lambda_0(\Gamma/\Gamma_0)^{2/3}\Delta^{-1}$. The overdensity field Δ from the Millennium simulation has been smoothed on a scale of 20 cMpc to calculate the spectra. The light blue shaded area represents a comoving size of $110 \text{ Mpc } h^{-1}$ and the corresponding effective optical depth in that chunk is shown in the lower right of each panel. The spectra are ordered from the lowest τ_{eff} for these chunks of $110 \text{ Mpc } h^{-1}$ to the highest from top to bottom. The lines of sight corresponds to those shown in Fig. 8 as labelled there and in the upper-left corner of each panel here. The spectra are calculated with $\beta_{\text{QSOs}} = 2$ and $\beta_{\text{gal}} = 1$ as in Fig. 8.

they reproduce the large opacity fluctuations with a hybrid DM semi-analytical model of ionization by (faint) galaxies only. Similarly to what we have done here in the last section, they assume a photoionization rate dependent mean free path. They show that with a rather low normalization of the mean free path, the mean free path in underdense regions where the emissivity drops can become very short. They further show that in this way moderate spatial fluctuations in the ionizing emissivity can be amplified into large-scale opacity fluctuations in reasonable agreement with those reported. Note, however, that the simulation technique of Davies & Furlanetto (2016) did not allow us to produce realistic mock absorption spectra and that the fluctuating Gunn–Peterson effect approximation was used instead. What also remains still to be seen is how realistic the very short assumed mean free paths in underdense regions are.

A further alternative explanation of the large opacity fluctuation has been recently proposed by D’Aloisio et al. (2015). These authors have argued that temperature fluctuations due to a spread of times when hydrogen reionization occurs could explain the large opacity fluctuations on large scales due to the temperature dependence of the recombination rate. Using also a hybrid technique based on high-resolution hydrosimulation combined with the excursion set formalism technique, D’Aloisio et al. (2015) showed that the patchy nature of reionization could lead to large-scale temperature fluctuations of sufficient amplitude. They also show that they can reproduce the reported τ_{eff} PDF, albeit with rather extreme assumption for the temperature of the IGM immediately after a patch is reionized. Reionization is however assumed to start early and to be rather extended, somewhat at odds with recent evidence for a rather late reionization (Choudhury et al. 2015; Planck

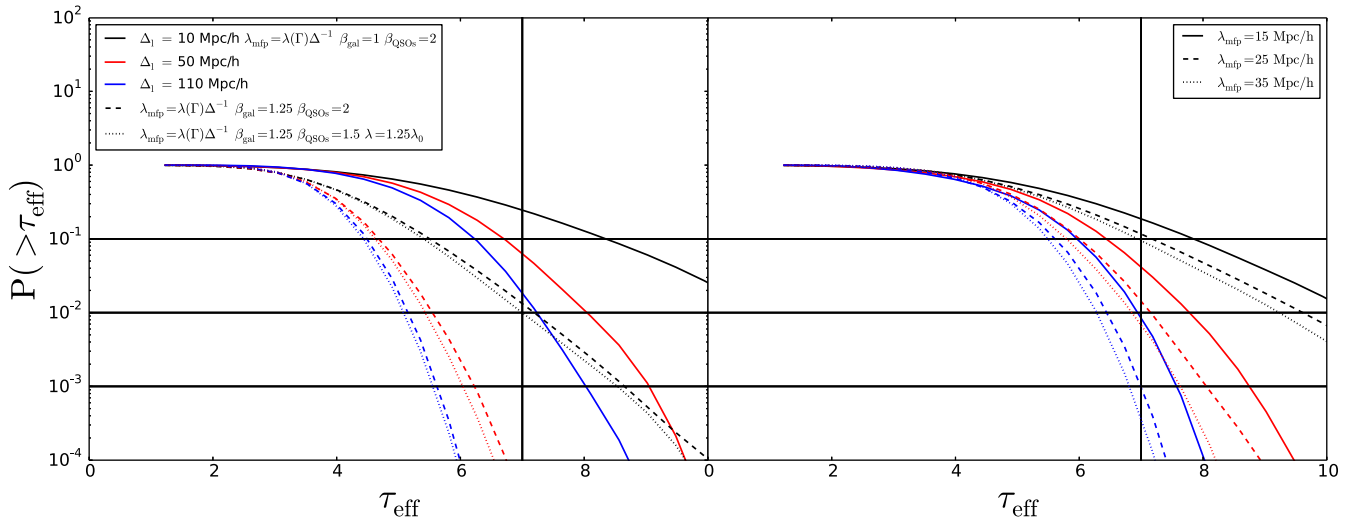


Figure 10. The cumulative effective optical depth PDF $P(>\tau_{\text{eff}})$ for chunks of spectra of different length ($\Delta_l = 10, 50, 110 \text{ Mpc } h^{-1}$ in black, red and blue, respectively) at $z = 5.8$ for different assumptions of the mean free path. The solid lines in the left-hand panel stand for the model with $\beta_{\text{QSOs}} = 2$ and $\beta_{\text{gal}} = 1$, the dashed lines for $\beta_{\text{QSOs}} = 2$ and $\beta_{\text{gal}} = 1.25$ and the dotted lines for $\beta_{\text{QSOs}} = 1.5$ and $\beta_{\text{gal}} = 1.25$ times the original value of the mean free path. The vertical black line corresponds to a value of $\tau_{\text{eff}} = 7$ as measured for the large trough of $110 \text{ Mpc } h^{-1}$ in the spectrum of ULAS J0148+0600 by B2015. The black horizontal lines show 10, 1 and 0.1 per cent.

Collaboration XIII 2016; Planck Collaboration XLVII 2016). D’Aloisio et al. (2015) furthermore neglect the effect of helium photoheating on the temperature (evolution) of the IGM and assume rather high temperatures (up to 30 000 K) immediately post-reionization.

In the late stages of preparing the manuscript for this paper, a preprint by Gnedin et al. (2016) appeared that found reasonable agreement between the τ_{eff} PDF in cosmological reionization simulations run as part of the CROC project. The simulations are similar to ours in terms of box size and resolution, but have only galaxies as ionizing sources. The main difference in how the τ_{eff} PDF was calculated appears to be that they have averaged simulations with a range of mean densities of their simulation box to take into account cosmic variance. This approach leads to rather different redshifts where the ionized regions percolate in the individual simulations from $z \sim 6.75$ to $z \sim 5.5$ (see Gnedin 2014 and Gnedin & Kaurov 2014 for comparison our simulations from Paper I overlap at about $z \sim 6$). Averaging over these different reionization histories drastically widens the PDF. We think this approach is rather problematic as it does not allow for ionizing radiation from sources in overdense regions to ionize underdense regions from the outside, and we think that this approach therefore will significantly overestimate the width of the τ_{eff} PDF. Unfortunately, simulations of larger regions with similar resolution as we have employed will be required to get to (more) converged results. Unfortunately at present we were not yet able to ‘afford’ the required dynamic range.

4.3 Correlations with other observables

As discussed in the last section, there are now three rather different suggestions for what is primarily responsible for the large reported opacity fluctuations at $z \sim 5.4\text{--}5.8$ on large scales. Gratifyingly, the different suggested explanations make rather different predictions for how the Ly α opacity correlates with other observables.

As already mentioned in the model discussed here regions of high transmitted flux should be correlated with the presence of QSOs near the line of sight (the transverse proximity effect, see Gallerani

et al. 2008). The detectability of this will depend on the QSO duty cycle and the angular distribution of the ionizing radiation. Better characterization of the QSO luminosity function in particular around its ‘knee’ will also help to determine the contribution of QSOs to the ionizing UV background and the opacity fluctuations at high redshift. Interesting in this regard is also the discovery of a rather large number of bright high-redshift galaxies with rather hard spectra (see Bowler et al. 2014; Bradley et al. 2014; Stark et al. 2015, 2017).

The model of Davies & Furlanetto (2016) predicts a very strong anticorrelation of the ionizing emissivity of galaxies with the long absorption troughs falling into large regions below the average ionizing emissivity. As already discussed, it also predicts a rather rapid decrease of the mean free path at $z > 5.5$ in particular in regions underdense in ionizing sources.

The observational signatures of the temperature fluctuation model of D’Aloisio et al. (2015) are less clear, but there should be a correlation rather than an anticorrelation between density field (smoothed on) on large scales and τ_{eff} as the overdense regions should be ionized earlier and should have more time to cool down to lower temperature leading to larger τ_{eff} . As already mentioned, this model predicts a rather early start of reionization.

There is of course the possibility that more than one of the effects discussed above contribute significantly to the opacity fluctuations on large scales. As already pointed out, the models of D’Aloisio et al. (2015) and Davies & Furlanetto (2016) predict opposite observational signatures. Therefore, we can imagine that if the two effects play an equivalent role, they could potentially cancel each other and might thereby not be able to explain the scatter in the τ_{eff} PDF.

Our model with AGNs does yet not take the temperature effects invoked by D’Aloisio et al. (2015) into account. We expect that the proximity zones of quasars will still be high-transmissivity regions when this is included. While hydrogen might reionize early there, these regions are likely nevertheless hot due to He II getting ionized there early as well. It is difficult to guess if the global shape of the effective Ly α opacity PDF would change or not. More sophisticated simulations including both galaxies and AGNs with a proper

treatment of the temperature evolution will be needed to answer this question.

The best way to test the additional effect of the fluctuating mean free path on large scales invoked by Davies & Furlanetto (2016) would be to run much larger simulations of reionization by galaxies to get a fair sampling of the voids and the related spatial distribution of the mean free path. For the AGNs, the model presented in this work already accounts in a simplified manner for the expected spatial fluctuation of the mean free path. However, a more accurate treatment of the modulation of the mean free path in a scenario where both AGNs and galaxies act as ionizing sources would require full multifrequency radiative transfer simulations in very large volumes, which is very difficult/not yet possible with current facilities at the desired resolution.

One interesting idea to disentangle the different scenarios would be to have a closer look to the line of sight of the quasar ULAS J0148+0600 that shows a very long ($110 h^{-1}$ cMpc) high optical depth Gunn–Peterson trough. The goal would be to measure the over/underdensity of galaxies in a cylinder around the trough to understand if high opacity regions are more prone to exhibit an excess or dearth of galaxies around them. The results could potentially give some constraints in regards to the model of Davies & Furlanetto (2016) and the one of D’Aloisio et al. (2015).

5 CONCLUSIONS AND OUTLOOK

We have combined here high-resolution full radiative transfer simulations with the large-volume Millennium simulation to model large-scale opacity fluctuations due to a significant contribution of QSOs to the UV background at $z \gtrsim 5$.

Our main results are as follows.

- (i) We can reproduce the reported broad distribution of the Ly α opacity on scales $\geq 50 h^{-1}$ cMpc with a contribution $\gtrsim 50$ per cent of QSOs to the ionizing emissivity.
- (ii) The ionizing emissivity of QSO required to reproduce the observed opacity depends rather sensitively on the assumed mean free path and its dependence on the local ionizing UV flux and overdensity.
- (iii) For assumptions, for the mean free path and its dependence suggested by our simulations, the required ionizing emissivity is similar to that predicted by the recent determination of the QSO luminosity function at this redshift by Giallongo et al. (2015).
- (iv) Our simulations neglect the increased temperatures around QSOs (primarily due to the reionization of He II), which will lead to correlated temperature and opacity fluctuations on large scales. Accounting for this should further reduce the ionizing emissivity due to QSOs required to explain the large opacity fluctuations on large scales.
- (v) Our simulations also reproduce very long ($110 h^{-1}$ cMpc) high optical depth Gunn–Peterson troughs like the one reported for ULAS J0148+0600, albeit rather rarely (in ~ 7 per cent of spectra).
- (vi) The model predicts a strong correlation of low Ly α opacity with the presence of QSOs close to the line of sight. This differs strongly from the predictions of alternative models that predict a strong correlation or anticorrelation of Ly α opacity with (over)density on large scales. The strength of the correlation should depend on the duty cycle as well as the the possible beaming of the QSOs.

Note, however, that the simulations presented here still suffer from their limited dynamic range. In particular, our high-resolution hydro/RT simulations while (marginally) resolving the Ly α opacity

(as well as the sinks of ionizing radiation) do not have a large enough simulation volume to comfortably capture the mean free path after percolation of the H II regions due to galaxies. Furthermore, the modelling of the QSO contribution to the ionizing UV background could only be done in post-processing with a rather simple model of the effect of QSOs on the mean free path. The modelling of alternative explanations for the reported large-scale opacity fluctuations, large-scale emissivity fluctuations of the galaxy ionizing emissivity and temperature fluctuations due to ‘patchy’ reionization suffers similar limitations.

Pushing our numerical simulations to higher dynamic range, i.e. larger volumes at comparable resolution and more sophisticated (full RT) modelling of the QSO contribution, including light travel effects for the QSO, exploring the effect of varying the angular distribution of their radiation and improved modelling of the photo-heating of hydrogen and in particular hydrogen with multifrequency RT simulations will be all important for improving the robustness of the predictions. This should, however, be well worth the effort, as it will allow us to infer much of what happened during the epoch of reionization from the fossil record present in Ly α forest data in the post-reionization epoch.

ACKNOWLEDGEMENTS

We thank Dominique Aubert for letting us use his code ATON and for helpful discussions. We also thank George Becker for helpful communication regarding his measurements of the flux PDF. We further thank James Bolton and Xiaohui Fan for helpful comments and suggestions. This work was supported by the ERC Advanced Grant 320596 ‘The Emergence of Structure during the epoch of Reionization’. This work was performed using the COSMOS and Darwin Supercomputers of the University of Cambridge High Performance Computing Service (<http://www.hpc.cam.ac.uk/>), provided by Dell Inc. using Strategic Research Infrastructure Funding from the Higher Education Funding Council for England and funding from the Science and Technology Facilities Council. This work furthermore used the Wilkes GPU cluster at the University of Cambridge High Performance Computing Service (<http://www.hpc.cam.ac.uk/>), provided by Dell Inc., NVIDIA and Mellanox, and part funded by STFC with industrial sponsorship from Rolls Royce and Mitsubishi Heavy Industries. Some of the hydrodynamical simulations used in this work were performed with supercomputer time awarded by the Partnership for Advanced Computing in Europe (PRACE) 8th Call. We acknowledge PRACE for enabling access to the Curie supercomputer, based in France at the Très Grand Centre de Calcul (TGCC). EP acknowledges support by the Kavli foundation. The research of JC and MH was supported by the Munich Institute for Astro- and Particle Physics (MIAPP) of the DFG cluster of excellence ‘Origin and Structure of the Universe’.

REFERENCES

- Aubert D., Teyssier R., 2008, MNRAS, 387, 295
- Aubert D., Deparis N., Ocvirk P., 2015, MNRAS, 454, 1012
- Baek S., Di Matteo P., Semelin B., Combes F., Revaz Y., 2009, A&A, 495, 389
- Becker G. D., Bolton J. S., 2013, MNRAS, 436, 1023
- Becker G. D., Bolton J. S., Haehnelt M. G., Sargent W. L. W., 2011, MNRAS, 410, 1096
- Becker G. D., Hewett P. C., Worseck G., Prochaska J. X., 2013, MNRAS, 430, 2067
- Becker G. D., Bolton J. S., Lidz A., 2015a, PASA, 32, e045

- Becker G. D., Bolton J. S., Madau P., Pettini M., Ryan-Weber E. V., Venemans B. P., 2015b, MNRAS, 447, 3402 (B2015)
- Boera E., Murphy M. T., Becker G. D., Bolton J. S., 2014, MNRAS, 441, 1916
- Bolton J. S., Haehnelt M. G., 2007, MNRAS, 382, 325
- Bolton J. S., Haehnelt M. G., 2013, MNRAS, 429, 1695
- Bolton J. S., Viel M., 2011, MNRAS, 414, 241
- Bolton J. S., Puchwein E., Sijacki D., Haehnelt M. G., Kim T.-S., Meiksin A., Regan J. A., Viel M., 2017, MNRAS, 464, 897
- Borthakur S., Heckman T. M., Leitherer C., Overzier R. A., 2014, Science, 346, 216
- Bouwens R. J., Illingworth G. D., Franx M., Ford H., 2007, ApJ, 670, 928
- Bouwens R. J. et al., 2015, ApJ, 803, 34
- Bowler R. A. A. et al., 2014, MNRAS, 440, 2810
- Bradley L. D. et al., 2014, ApJ, 792, 76
- Calverley A. P., Becker G. D., Haehnelt M. G., Bolton J. S., 2011, MNRAS, 412, 2543
- Chardin J., Aubert D., Ocvirk P., 2012, A&A, 548, A9
- Chardin J., Aubert D., Ocvirk P., 2014, A&A, 568, A52
- Chardin J., Haehnelt M. G., Aubert D., Puchwein E., 2015, MNRAS, 453, 2943 (Paper I)
- Choudhury T. R., Puchwein E., Haehnelt M. G., Bolton J. S., 2015, MNRAS, 452, 261
- Ciardi B., Ferrara A., 2005, Space Sci. Rev., 116, 625
- D'Aloisio A., McQuinn M., Trac H., 2015, ApJ, 813, L38
- D'Aloisio A., Upton Sanderbeck P. R., McQuinn M., Trac H., Shapiro P. R., 2016, MNRAS, preprint ([arXiv:1607.06467](#))
- Davies F. B., Furlanetto S. R., 2016, MNRAS, 460, 1328
- Dijkstra M., Wyithe S., Haiman Z., Mesinger A., Pentericci L., 2014, MNRAS, 440, 3309
- Fan X. et al., 2006, AJ, 132, 117
- Finkelstein S. L. et al., 2015, ApJ, 810, 71
- Fotopoulou S. et al., 2016, A&A, 592, A5
- Gallerani S., Ferrara A., Fan X., Choudhury T. R., 2008, MNRAS, 386, 359
- Georgakis A. et al., 2015, MNRAS, 453, 1946
- Giallongo E. et al., 2015, A&A, 578, A83
- Gnedin N. Y., 2014, ApJ, 793, 29
- Gnedin N. Y., Kaurov A. A., 2014, ApJ, 793, 30
- Gnedin N. Y., Becker G. D., Fan X., 2016, ApJ, preprint ([arXiv:1605.03183](#))
- Grazian A. et al., 2016, A&A, 585, A48
- Haardt F., Madau P., 2012, ApJ, 746, 125 (HM2012)
- Haardt F., Salvaterra R., 2015, A&A, 575, L16
- Hopkins P. F., Richards G. T., Hernquist L., 2007, ApJ, 654, 731
- Hui L., Gnedin N. Y., 1997, MNRAS, 292, 27
- Iliev I. T., Mellema G., Pen U., Merz H., Shapiro P. R., Alvarez M. A., 2006, MNRAS, 369, 1625
- Jiang L. et al., 2009, AJ, 138, 305
- Kimm T., Cen R., 2014, ApJ, 788, 121
- Kimm T., Katz H., Haehnelt M., Rosdahl J., Devriendt J., Slyz A., 2016, MNRAS, preprint ([arXiv:1608.04762](#))
- Kulkarni G., Hennawi J. F., Oñorbe J., Rorai A., Springel V., 2015, ApJ, 812, 30
- Leethochawalit N., Jones T. A., Ellis R. S., Stark D. P., Zitrin A., 2016, ApJ, 831, 152
- Leitherer C., Hernandez S., Lee J. C., Oey M. S., 2016, ApJ, 823, 64
- Lidz A., McQuinn M., Zaldarriaga M., Hernquist L., Dutta S., 2007, ApJ, 670, 39
- Ma X., Kasen D., Hopkins P. F., Faucher-Giguère C.-A., Quataert E., Kereš D., Murray N., 2015, MNRAS, 453, 960
- McQuinn M., 2016, ARA&A, 54, 313
- McQuinn M., Oh S. P., Faucher-Giguère C.-A., 2011, ApJ, 743, 82
- Madau P., Haardt F., 2015, ApJ, 813, L8
- Madau P., Haardt F., Rees M. J., 1999, ApJ, 514, 648
- Matsuoka Y. et al., 2016, ApJ, 828, 26
- Meiksin A. A., 2009, Rev. Mod. Phys., 81, 1405
- Miralda-Escudé J., Haehnelt M., Rees M. J., 2000, ApJ, 530, 1
- Mostardi R. E., Shapley A. E., Steidel C. C., Trainor R. F., Reddy N. A., Siana B., 2015, ApJ, 810, 107
- Ocvirk P. et al., 2016, MNRAS, 463, 1462
- Pawlak A. H., Schaye J., Dalla Vecchia C., 2015, MNRAS, 451, 1586
- Planck Collaboration XIII, 2016, A&A, 594, A13
- Planck Collaboration XLVII, 2016, A&A, preprint ([arXiv:1605.03507](#))
- Puchwein E., Springel V., 2013, MNRAS, 428, 2966
- Rahmati A., Pawlik A. H., Raičević M., Schaye J., 2013, MNRAS, 430, 2427
- Rahmati A., Schaye J., Bower R. G., Crain R. A., Furlong M., Schaller M., Theuns T., 2015, MNRAS, 452, 2034
- Reddy N. A., Steidel C. C., Pettini M., Bogosavljević M., Shapley A., 2016, ApJ, 828, 1018
- Robertson B. E. et al., 2013, ApJ, 768, 71
- Robertson B. E., Ellis R. S., Furlanetto S. R., Dunlop J. S., 2015, ApJ, 802, L19
- Rorai A., Hennawi J. F., White M., 2013, ApJ, 775, 81
- Rosdahl J., Blaizot J., Aubert D., Stranex T., Teyssier R., 2013, MNRAS, 436, 2188
- Shapley A. E., Steidel C. C., Strom A. L., Bogosavljević M., Reddy N. A., Siana B., Mostardi R. E., Rudie G. C., 2016, ApJ, 826, L24
- Siana B. et al., 2015, ApJ, 804, 17
- Songaila A., Cowie L. L., 2010, ApJ, 721, 1448
- Springel V. et al., 2005, Nature, 435, 629
- Stark D. P. et al., 2015, MNRAS, 454, 1393
- Stark D. P. et al., 2017, MNRAS, 464, 469
- Telfer R. C., Zheng W., Kriss G. A., Davidsen A. F., 2002, ApJ, 565, 773
- Teyssier R., 2002, A&A, 385, 337
- Theuns T., Leonard A., Efstathiou G., Pearce F. R., Thomas P. A., 1998, MNRAS, 301, 478
- Theuns T., Mo H. J., Schaye J., 2001, MNRAS, 321, 450
- Vanden Berk D. E. et al., 2001, AJ, 122, 549
- Viel M., Becker G. D., Bolton J. S., Haehnelt M. G., 2013, Phys. Rev. D, 88, 043502
- Wise J. H., Demchenko V. G., Halicek M. T., Norman M. L., Turk M. J., Abel T., Smith B. D., 2014, MNRAS, 442, 2560
- Worseck G. et al., 2014, MNRAS, 445, 1745
- Wyithe J. S. B., Bolton J. S., 2011, MNRAS, 412, 1926
- Wyithe J. S. B., Bolton J. S., Haehnelt M. G., 2008, MNRAS, 383, 691
- Xu H., Wise J. H., Norman M. L., Ahn K., O'Shea B. W., 2016, ApJ, preprint ([arXiv:1604.07842](#))
- Yoshiiura S., Hasegawa K., Ichiki K., Tashiro H., Shimabukuro H., Takahashi K., 2016, MNRAS, preprint ([arXiv:1602.04407](#))

APPENDIX A: THE VARYING MEAN FREE PATH

In Section 2.3.2, we had discussed our modelling of the mean free path. Here, we show in more detail how the photoionization rate as well as the mean free path vary spatially in our different models. The case of a constant mean free path is compared to our models where the mean free path depends on the local value of Γ_{12} as a power law (see Davies & Furlanetto 2016)

$$\lambda_{\text{mfp}}(\Gamma) = \lambda_0(\Gamma / \Gamma_0)^{2/3} \Delta^{-\gamma} \quad (\text{A1})$$

We have considered two different values of γ to test the dependence of the mean free path on local overdensity. First, we tested $\gamma = 1$ as in Davies & Furlanetto (2016) and then we also investigated models with $\gamma = 0.4$, which is the value we found in our simulations.

We note here that we used the DM overdensity from the Millennium simulation to estimate Δ and that we have smoothed the density field with a 20- and 5-cMpc-wide top-hat filter. Davies & Furlanetto (2016) have argued that such a coarse resolution is sufficient (they have used 5 cMpc) as it resolves the typical mean free path at the considered redshifts. We find very little differences by smoothing the field on scales of 5 or 20 cMpc.

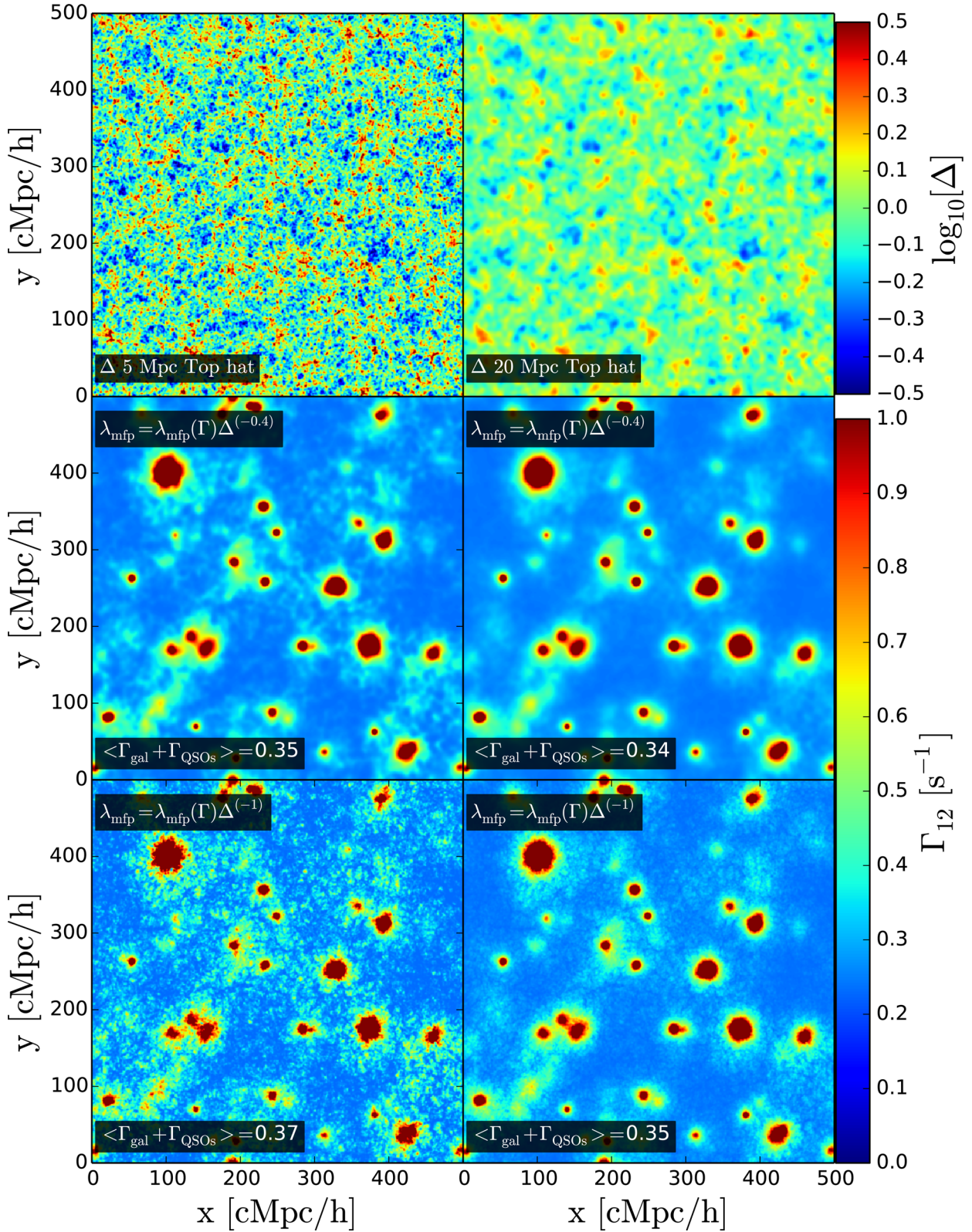


Figure A1. The spatial distribution of the photoionization rate Γ_{12} in a slice of $976.5625 \text{ cMpc } h^{-1}$ in our different models with the luminosity function of Giallongo et al. (2015). The left-hand column shows the case for the density field Δ smoothed with a 5-cMpc-wide (top-left panel) top-hat filter and 20-cMpc-wide top-hat filter (top-right panel). The second row shows Γ for an overdensity dependence of the mean free path $\propto \Delta^{-0.4}$ while the bottom row is for Δ^{-1} .

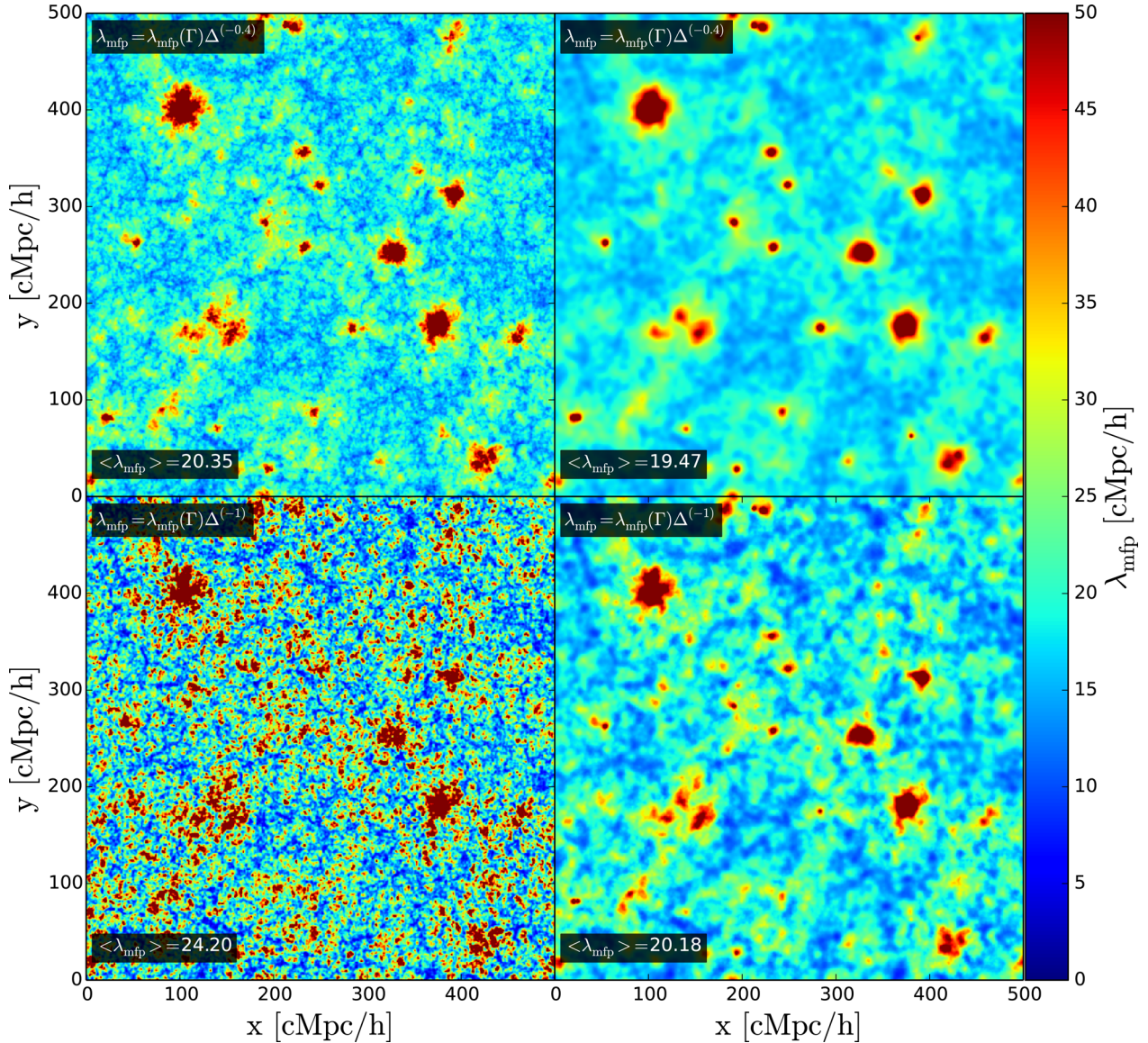


Figure A2. The spatial distribution of the mean free path λ_{mfp} for our different models with the luminosity function of Giallongo et al. (2015). The left-hand column shows the case in which the density field Δ has been smoothed on a 5-cMpc scale while the right-hand column is based on the 20 cMpc smoothing. The top row shows Γ for an overdensity dependence of the mean free path $\propto \Delta^{-0.4}$ while the bottom row is for Δ^{-1} .

Fig. A1 shows the spatial distribution of Γ_{12} for our four different models tested. For illustrative purposes, we also show the overdensity field smoothed with a 5- or 20-cMpc-wide filter in the two upper panels. Overall, the power law dependence with overdensity of the mean free path as well as the smoothing adopted for the overdensity field only have a small effect on the global photoionization rate field. A higher granularity is found when smoothing with the 5-cMpc-wide filter compared to the 20-cMpc-wide filter, but similar values of $\langle \Gamma \rangle$ are found whatever the assumed power-law index for the overdensity dependence of the mean free path. Raising the power -law index from 0.4 to 1 changes the average value of $\langle \Gamma \rangle$ for both smoothing scales only very moderately.

The same is true for the spatial distribution of the mean free path itself shown in Fig. A2. A smaller value of the smoothing scale of 5 cMpc and a steeper dependence of overdensity with $\gamma = 1$ lead to a slightly larger average value of the mean free path compared to the other cases. But this small difference in the global mean free path translates only to rather small changes in the photoionization rate maps, which in turn only moderately change the τ_{eff} PDF as seen in Section 3.3.

This paper has been typeset from a TeX/LaTeX file prepared by the author.